JCU ePrints

This file is part of the following reference:

Page, Geoff (2007) ***Mass Transport Evaluation using consolidated VHF Radar and Acoustic Doppler Current Profiler data.*** **Masters (Research) thesis, James Cook University.**

Access to this file is available from:

http://eprints.jcu.edu.au/2085

JCU
JAMES COOK UNIVERSITY

1. Introduction

To fully evaluate the mass transport (or volume transport) of a coastal ocean flow requires the measurement of current velocities throughout the horizontal and vertical dimensions of the flow. A variety of current measurement technologies exists for the measurement of ocean currents, such as Vector Averaging Current Meters, Acoustic Doppler Current Profilers, Electromagnetic Current Meters, and Ocean Surface Current Radar Systems. Each of these instruments has limitations as to its coverage of measurement, and each, used individually, cannot provide a complete set of current measurements for the purposes of estimating mass transport. With the exception of an Ocean Surface Current Radar system, these instruments obtain current measurements only at a single geographic location. Unless many sensors are deployed, single point measurements have no capability to measure currents across the width of a coastal flow or inlet, or of surface currents accurately. Although the radar system can provide current measurements over a larger geographic area, the measurements obtained are only of surface currents. In order to obtain the most complete evaluation of current velocities in an ocean flow, it is proposed that a combination of current sensing instruments be used.

The aim of this research is to establish a more complete method of evaluating mass transport through a coastal inlet using the combination of data from two of the most advanced current measurement technologies. The two instruments to be used are an Acoustic Doppler Current Profiler and the PortMap Ocean Surface Current Radar.

1.1 Overview of the Thesis

Starting with an investigation into evaluating mass transport, Chapter 2 examines the literature concerning the estimation of mass transport in a coastal flow. This includes an investigation into the measurements required for mass transport together with models for the analysis of surface boundary and bottom boundary regions of the flow. The measurement technologies considered most suitable for this purpose, the Acoustic Doppler Current Profiler and the Ocean

Surface Current Radar are also described with regards to their operation, advantages, limitations and measurement characteristics. Current research into the effective combination of ADCPs and Ocean Radar systems for the profiling of coastal currents is also presented.

Chapters 3 and 4 describe the experiment to be carried out, together with a detailed technical look at the instruments used and how they were deployed. Chapter 3 presents the design of the experiment to be carried out with a description of the site in Italy where these instruments were deployed at the Lido Channel entrance to the Venice Lagoon. The significance of why this particular site was chosen is discussed, together with an outline for the acquisition of additional data from existing local Tide, Wind and Meteorological instruments. The selection of ADCP used and the details of how it was deployed within the channel is also described. Chapter 4 presents a thorough investigation into the design and specifications of the PortMap Radar system and how the returned radio signals are analysed to produce surface current measurements using this system. Furthermore the deployment of each radar station at locations on the seawalls either side of the Lido Inlet is explained in detail.

Chapter 5 presents the data analysis methods used, and the results obtained using these methods. The chapter begins by investigating the quality of the data obtained by all the instrumentation used. This is followed by the process used to analyse raw radar data obtained by the PortMap Radar system, together with the techniques used to generate secondary current data. Two different techniques for obtaining radial current measurements from radar spectra are described together with the methods used to generate secondary current data and complete transect profiles. Following the discovery of a system fault, the final section in this chapter shows how the analysis method was modified to address this fault. The re-analysis produced higher resolution vector current maps, though at reduced range.

Chapter 6 details some key observations made during the data analysis process. The first of these was the observation of a tidal phase difference between the Sabbioni and Lido sides of the Lido Inlet. Also presented is the detection by the PortMap Radar of breaking wave backwash currents in the first range cell at the Lido station. Furthermore the effect of high velocity surface currents that could perceivably be out of the measurement range of the PortMap radar is investigated.

Chapter 7 provides an overview of the results obtained together with the major points highlighted in Chapter 6. Suggestions for how the techniques of evaluating mass transport using combined radar and ADCP data may be further developed are also given.

2. Literature Review

2.1 Mass Transport Estimation and Current Measurement

In estimating the mass transport of water, we are concerned with the total volume (or mass) of water that has passed through a given cross section area. In order to accurately estimate the mass transport of water through an estuarine inlet, the measurement and analysis of the current flow passing through the cross sectional area of the inlet are required.

2.1.1 Mass Transport Integral and Boundary Layer Velocity Distribution

The volume transport across the transect of a coastal inlet is simply the integral of the velocity over the cross sectional area. The units of this measurement are m^3/s. In order to calculate the mass transport through the same area, we integrate the product of density and velocity over this area, measured in kg/s. A further calculation regarding mass transport where the tidal current is dominant, is that of residual flow. This is obtained by averaging the current over many tidal periods. If the flow is averaged over weeks or months, residual currents in the form of wind-driven current, density-driven current or tide-induced current become apparent (Yanagi, 1999).

The difficulty in calculating mass transport with any degree of precision is in obtaining accurate knowledge of the water velocity throughout the entire cross sectional area of the inlet. River discharge, tidal forcing and wind each have an influence on the mass transport through an estuarine inlet, and the effect that these have can be influenced by bathymetry, coastal structures and sea floor characteristics. Friction between the water flow and the solid boundary of the sea floor causes the water velocity to be reduced. This velocity reduction is more pronounced near the sea bed than further up in the flow and this variation is characterised by a logarithmic boundary layer velocity profile (Dyer, 1986).

There are some variations to the profile depending on the stability of the density profile, but for a stable layer and assuming the mixing length is linear with z such that

$$l(z) = \kappa z \tag{2.1}$$

The logarithmic profile is then described by the von Karman-Prandtl equation

$$u = \frac{u*}{\kappa} \ln \frac{z}{z_0} \tag{2.2}$$

where $u*$ is the friction velocity of the flow estimated from a measured velocity profile, z is the height above the sea bed, κ is von Karman's constant (0.41) and z_0 is generally known as the roughness length and explicitly allows for varying roughness of the sea bed (Soulsby, 1983). Current velocity measurements obtained throughout a vertical column of water can be used to determine the parameters of this equation and to define the vertical structure of the current flow. In shallow water, this boundary layer velocity profile may be present across the entire depth of water or it may be limited by density layers, temperature layers or wind-driven currents within the water column.

2.1.2 Enhanced Surface Current Shear - Wind Effects and Density Layers

The effect of wind blowing across a surface of water causes a wind stress on the surface layer which in turn causes wind driven surface currents to form (Yanagi, 1999). The wind induced surface current causes shear stress on lower layers of water. This creates a logarithmic boundary layer velocity profile similar to that of the sea bed boundary layer. In an investigation into wind-driven surface currents, Fernandez et al (1996) characterised this by the following equation :-

$$\frac{U_s - U_x(z)}{u_w*} = \frac{1}{\kappa} \ln \frac{z}{z_0} + 8.5 \tag{2.3}$$

where $U_x(z)$ is the velocity of the water at some depth, z, U_s is the value of the current at the surface, u_w* is the friction velocity at the surface of the water, κ is von Karman's constant, and z_0 is the roughness length. In similarity to the sea-bed boundary layer profile, accurate velocity measurements of the surface current and within deeper layers are required to determine the parameters u_w*

and z_0. The constant given as 8.5 depends on drag coefficient, and is also determined experimentally for a given situation.

Density layers can also affect the current structure within the vertical column of water. River water entering an estuary can partially mix with the salt water and will eventually flow out to the open sea in a less dense top layer of water. Sea water will also flow into the estuary below this upper layer to balance this circulation. Although river flow into the estuary tends to reduce the salinity, a corresponding inflow of sea water tends to balance this to a point of equilibrium (Pickard, 1990). Currents in layers of unlike density will differ as a result of this process, and their presence will have some effect on the logarithmic boundary velocity profiles from the sea bed and the sea surface.

If any of these dynamic processes in the estuarine environment are to be clearly accounted for in the calculation of mass transport of water through an inlet, scientific tools are required to accurately measure the current velocity at points throughout the entire cross sectional area of the inlet. Acoustic Doppler Current Meters and Ocean Surface Current Radar systems are considered the two most modern and capable technologies that are available for this purpose.

2.2 Acoustic Doppler Current Meters

An Acoustic Doppler Current Profiler (ADCP) is an instrument for measuring current velocity that uses acoustic pulses and the Doppler effect to obtain velocity measurements throughout a column of water. This instrument was originally adapted from commercial speed logs used in ships as these tracked the ship's speed over ground or speed through the water using sonar technology. The ADCP was developed from this sonar technology and was first commercially available in the latter half of the 1970s (Rowe and Young, 1979). The first commercially available ADCPs were designed to measure water velocity with greater accuracy and to allow the current to be measured in cells throughout the vertical column of water. Modern ADCPs are available in a variety of operating frequencies depending on operating circumstances and can

be ship based, surface mounted or bottom mounted. The use of ADCPs in the measurement of geophysical current flow is now well established (e.g., Lee, 2002; Wewetzer, 1999). Research into the extraction of wave, wind and sediment concentration data from ADCP measurements has also been investigated by various researchers (e.g., Kostaschuk, 2005; Zedel, 1995; Schott, 1989). Of primary importance, the ADCP is able to provide measurements of the vertical structure of current flow. This structure can be clearly seen in the sequence of measurements depicted in Figure 2.1 from a study undertaken by Lueck and Lu (1997). This study investigated the logarithmic boundary layer in a tidal channel.

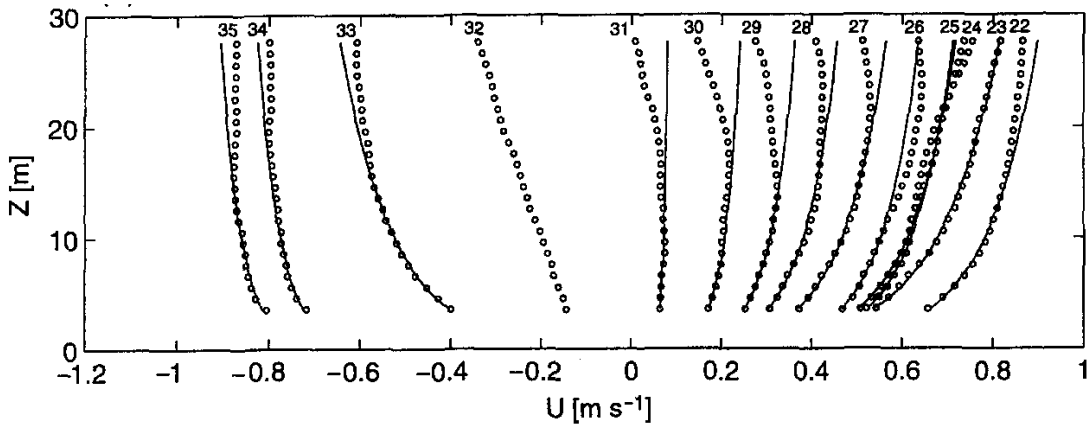

Figure 2.1 - Logarithmic Profiles obtained from ADCP Measurements
Sequence numbers identify each sequential 20 minute sampling period.
o - ADCP Measurement, Solid line - logarithmic profile model fit
(Lueck and Lu, 1997)

2.2.1 Principles of Operation

The Acoustic Doppler Current Profiler uses the Doppler effect to determine the velocity of suspended particles such as plankton and sediment in the water column. Critical assumptions in the use of ADCPs is that the scattering particles are presumed to be travelling at the same average velocity as the surrounding water and that the water velocity is constant within horizontal layers. The ADCP measures the velocity of the scattering particles by transmitting acoustic pulses and then analysing the signals of the subsequent reflections from these particles.

Velocity

The sound waves reflected from the scatterers are Doppler shifted in frequency relative to the particles' velocities. The velocity of the water can thus be determined from the following formula describing the Doppler effect, which describes the shift in sound frequency received from a moving scatterer:

$$F_d = 2 * F_s(V/c) \tag{2.4}$$

where V is the relative velocity of the source and receiver, F_d is the resultant Doppler shift, F_s is the frequency of the transmitted pulse and c is the speed of sound.

Velocity Direction

To enable the instrument to determine the velocity of the water in three dimensions, three (120˚ horizontal spacing) or four (90˚ horizontal spacing) orthogonal transducers and corresponding sound beams are used to resolve measurements in all directions of motion. These beams are typically aligned between 20˚ to 30˚ from the vertical. If four orthogonal transducers are used, the fourth redundant measurement is used to produce a measurement of error velocity. The average of the vertical velocity from two opposing beam pairs is used to calculate the vertical water velocity. The difference between the two opposing beam pairs is known as the error velocity measurement and is used to investigate the error of the measurements obtained.

Range

In order to produce a vertical profile of current velocities, the water column under investigation is broken into regularly spaced depth cells, called bins. Time based range-gating is used to separate the returned echo data into their bins related to their distance from the instrument.

2.2.2 Advantages, Limitations and Sources of Error

The variety of deployment methods is a distinct advantage of the ADCP, as is their ability to provide multiple points of measurement within the water column.

Commonly deployed on the sea bed, moored at the surface or moored at some depth in between, ADCPs can be self-contained or directly linked to recording stations to monitor data in real-time. When self-contained, ADCPs are limited in their deployment period by battery capacity and data storage capacity. If they are linked to a recording station to overcome these issues or to provide real-time data, the duration of their deployment is then limited by the growth of fouling marine organisms (barnacles) on the transducers. ADCP mountings within a frame on the sea bed must be carefully designed to avoid obstruction of trawling vessels which can result in corruption of data or loss of instruments (Dessureault, 1991). If it is not possible to deploy a fixed ADCP in a given situation for an extended time, advances in Global Positioning Systems (GPS) and sea floor tracking have also allowed their accurate use aboard boats. This enables current profile measurements to be made along coastal transects, such as in the study conducted by Lee (2002). Similarly, a towed, surface-mounted ADCP was used by Cheng and Gartner (2003) to profile cross-sectional river flows.

Unlike single point measurement devices such as mechanical rotors or electromagnetic sensors, ADCPs have the advantage that they are able to obtain current measurements throughout the vertical column of water (Lane, 1999). The water column is divided into depth cells (or bins) with weighted average measurements obtained throughout the cell. This weighted average technique places greater importance on the measurements obtained closer to the centre of the depth bin than those toward the edges.

Unfortunately, ADCPs have the disadvantage that the results become unreliable at measurement boundaries such as the sea surface or sea bed (depending on deployment orientation). This is due to the contamination of faint signals from particle echoes by the stronger sound reflections from these reflective boundaries. This is known as side-lobe contamination, as it is the transmission

and reception by the transducer's side-lobes that gives the acoustic reflections from the boundaries. The RD Instruments, Principles of Operation Primer (1996) details the -3dB beamwidth of a typical 1200 kHz ADCP to be 1.4˚, with a single direction side-lobe level of -42dB at approximately 30˚ from the axis. For an ADCP with beam angles of 30˚ from the vertical, this side-lobe is presented directly toward the surface or bottom boundary, as can be seen in Figure 2.2.

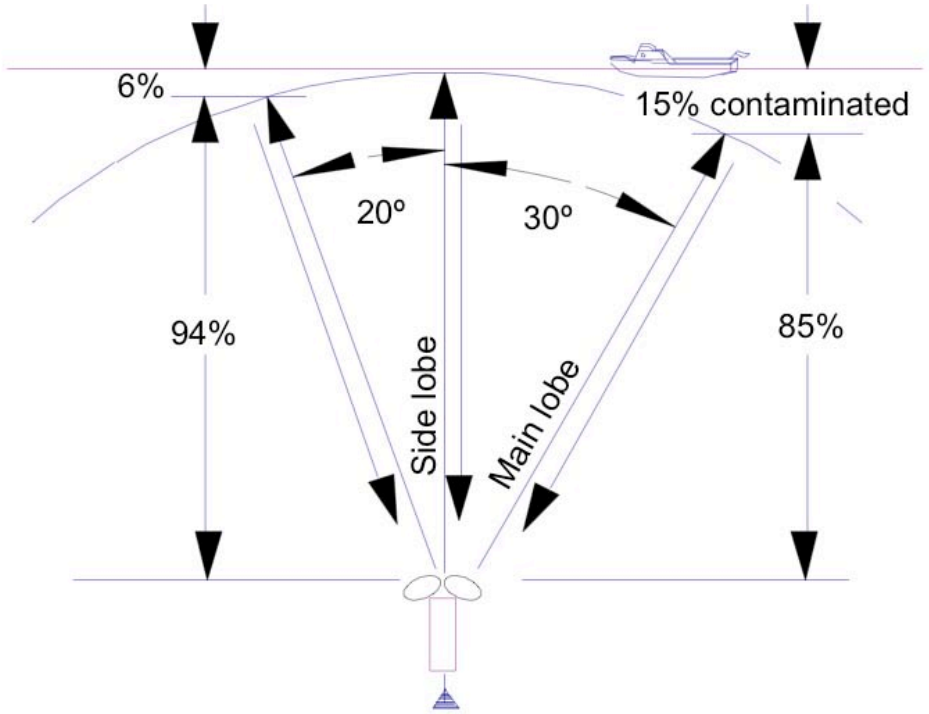

Figure 2.2 - The relationship between ADCP transducer beam angle and the thickness of the contaminated layer at the surface. (RD Instruments, Principles of Operation Primer, 1996)

Any range with side-lobes presented to a boundary will cause measurements to be biased towards zero. This effect is well documented by Apell (1991) where a study investigated the use of various baffles to reduce unwanted effects from side-lobe contamination in ADCPs. The usable range of an ADCP deployment is characterised by the following equation where R_{max} is the usable range, D is the depth of deployment and θ is the beam angle relative to the vertical (RD Instruments, Principles of Operation Primer, 1996).

$$R_{max} = D\cos(\theta) \tag{2.5}$$

In a typical bottom mounted ADCP deployment in 20 m of water with 20˚ beams, this will result in side-lobe contamination in the top 1.21 m of water. Changes in depth and sea surface roughness caused by tidal variation and waves can cause further contamination of data to a bottom mounted ADCP looking toward the surface. Similarly, a surface or ship-mounted ADCP over rough seabed topography can produce the contamination of data for some of the lowest bins (Kostaschuk et al., 2005). Other causes of data contamination or discontinuities can exist in tidal regions where data bins are periodically out of the water. A new instrument in the measurement of river flow, a surface mounted BoogieDopp Current Profiler has been used in a study by Cheng and Gartner (2003) to provide current profiling to within 11cm of the surface. This particular instrument seemed to overcome some of the previous limitations in measuring velocities close to the surface in rivers.

Contamination of measurements can also be caused by acoustic ringing that occurs following the transmission of a sound pulse by the instrument. The source of this acoustic ringing can be attributed to receiving electronics, protective covers, bed frames or ships' hulls and can generate a zero bias of measurements, as the received signal is not Doppler shifted. Extensive errors in measurements in the first data bin close to the sea floor were discarded in a study by Tang (1994) due to ringing of a protective cover. It was also discovered in the subsequent data analysis that data in bins 2 and 3 were of lowered accuracy for this same reason. Also in this study by Tang, the furthest bin within the usable range was rejected due to the reflection of side-lobe energy from the bottom of waves.

Aside from the above limitations leading to the severe corruption of data, error and uncertainties exist in the recorded data due to random error and measurement bias. Bias is typically found to be less than 10^{-2} $m.s^{-1}$ and is dependent on many environmental factors and internal operating specifications (RD Instruments, Principles of Operation Primer, 1996). The magnitude of random error depends on internal attributes such as sound frequency, bin size and beam pattern or it may be influenced by environmental factors such as turbulence, internal waves or from movement of the ADCP itself. In modern

broadband ADCPs, random error can be reduced by averaging the returned data over a number of ping cycles to the point where its effect becomes less than the effect of measurement bias. The amount of random error can be estimated by calculating the standard deviation of the velocity error measurement, obtained through the use of four measuring beams. The velocity error measurement is also used to reliably test whether the water velocity is constant within horizontal layers, i.e. is of horizontal homogeneity. In-homogeneous flows tend to cause large error velocities and unreliable data. Turbulent coastal flows do not generally satisfy the assumption of homogeneous flow as the velocity is never homogenous over the span of the beams, and further data processing is required to obtain useful velocity profiles (Lu and Lueck, 1999).

Errors can also be caused by the lack of sufficient reflecting particles in the water. Lane (1999) found that these can occur on a seasonal time scale where there are not enough biological scatterers present in portions of the water column to obtain accurate measurements.

2.2.3 Obtainable Measurements and their Characteristics

The primary results obtained from ADCPs are temporally averaged velocity measurements that are weighted over a range cell for various points throughout the column of water. Parameters obtained from these ADCP measurements are those relating to the distribution of velocity within this vertical column. Mass transport can be directly estimated from such velocity distributions and can be related to logarithmic profiles to obtain boundary layer parameters (Smith, 2002; and Lueck and Lu ,1997). Other research using vessel mounted ADCPs to investigate mean river flows has suggested that average velocities and turbulence intensities can also be accurately estimated (Muste, 2004).

It has been shown that surface parameters such as wave particle velocity (Apell, 1991) and significant wave height (Rowsell, 2002) can be determined from ADCP data. Additionally, bottom tracking capabilities and returned back-scatter signal strength have been used in sediment dynamics studies to estimate parameters such as bed load and suspended load (Kostaschuk, 2005). Furthermore, Schott (1989) reported a correlation between returned echo amplitude from the surface and wind strength. This has again been revisited by studies in monitoring sea surface conditions using ADCPs by Visbeck and Fischer (1995) and Zedel et al. (1995).

2.2.4 Application to a coastal inlet for the estimation of mass transport

For an ADCP instrument to be deployed over a month long time period on the sea bed of a shallow channel, it is of key concern how the instrument should be best configured to give the most accurate data over the greatest range of depth. Primary factors affecting the usable range of measurements are ringing distance and the amount of side-lobe contamination from boundary layers. The effect of ringing is reduced by the blanking of measurements in short ranges near to the instrument. To reduce the ringing distance to a minimum proportion of the depth in a shallow channel, a ping frequency of 600 kHz or 1200 kHz should be used (Table 1, RD Instruments, Principles of Operation Primer, 1996). To reduce the amount of contamination from side-lobes an ADCP with beam

angles of 20˚ should be used . RD Instruments specifies the 1200 kHz ADCP as having a range of 25 m and power consumption of 15 W (Table 2, RD Instruments, Principles of Operation Primer, 1996). Studies of currents in shallow regions to have used an ADCP operating at a frequency of 1200 kHz and 20˚ beam angles include those performed by Cheng et al. (2003) and Rowsell et al. (2002).

Frequency	Ringing distance
75 kHz	6 m
150 kHz	4 m
300 kHz	2 m
600 kHz	1 m
1200 kHz	0.5 m

Table 1.1 Typical ringing times expressed as distances from the transducers. Speed of sound approx. 1467 m.s^{-1} (at 4˚C, 35‰ salinity and at sea level) (RD Instruments, Principles of Operation Primer, 1996)

Frequency (kHz)	α(dB/m)	Nominal Range (m)	@ Power (W)
76.8	0.022-0.028	700	250
153.6	0.039-0.050	400	250
307.2	0.062-0.084	120	80
614.4	0.14-0.20	60	30
1228.8	0.44-0.66	25	15

Table 1.2 Sound absorption (At 4˚C, 35‰ salinity and at sea level) and nominal profiling range of a Broadband ADCP. The transmit power listed is the maximum power that can be transmitted subject to limitations caused by shock formation. (RD Instruments, Principles of Operation Primer, 1996)

2.3 VHF / HF Coastal Ocean Surface Current Radar

Coastal Radar systems provide a remote sensing alternative to the measurement of ocean surface currents. Unlike in-situ current meters such as ADCPs, Coastal Radar can provide vector maps representing surface currents over large areas of ocean, or high spatial resolution current mapping over smaller areas such as coastal inlets or channels. Coastal Radar systems exist that operate in the High Frequency (HF) band between 3 - 30 MHz and the Very High Frequency (VHF) band between 30 - 300 Mhz.

2.3.1 Principles of Operation

Doppler Radar Systems were originally developed for military use as a means of aircraft detection whereby a transmitted electromagnetic signal would be reflected by a moving aircraft. This reflected radar signal would be Doppler shifted in frequency relative to the radial velocity of the aircraft. Although not clearly understood at the time, high levels of noise or back-scatter related to sea state were often observed with the use of these systems over coastal seas such as the English Channel. Structure in this “sea clutter” was first identified and characterised by Crombie (1955) where he correctly related this back-scatter to ocean waves of half the wavelength of the transmitted radar signal. His analysis of the returned spectrum identified a Doppler shift related to the phase velocity of these waves toward or away from the observing radar. Theoretical first order verification of this observed back-scatter determined to be “Bragg Scatter” was later performed by Barrick (1972a) who further proposed its usefulness in the implementation of wave sensing and sea state sensing (Barrick et al., 1972b). The application of Doppler radar to the measurement of surface current was not realised until Stewart and Joy (1974) detailed a method of extracting surface current data from the observed back-scatter spectrum. From a comparison between observed phase velocity of the scattering waves and the theoretical phase velocity these deep water waves would have in still water, they were able to deduce the underlying surface current at the observed point. Experimental comparisons with drifting drogues verified the accuracies of

their results to within a few centimetres per second. This technique of measuring surface current was further developed by Barrick (1977) in the use of two observing High Frequency (HF) radar units to produce current vector maps covering an area of over 2000 km^2 and to a distance 70 km offshore. As each individual radar unit provides only the radial component of the current velocity toward or away from the observing radar, two radar stations located a few tens of kilometres apart are used to resolve the two-dimensional current velocity vector. His use of this technique provided two dimensional surface current maps for the region under investigation.

Radial Component of Current Velocity

As described earlier, the total Doppler shift of the observed back-scatter is a result of the Doppler shift from the scattering waves' phase velocity and the underlying surface current. As detailed by Barrick et al. (1977), this total Doppler shift, f_D can be represented as the sum of a component due to Bragg wave phase velocity, f_B and an additional component,
Δf as follows :-

$$f_D = f_B + \Delta f \tag{2.6}$$

$$f_D = \pm\sqrt{\frac{g f_0}{\pi c}} - 2\ f_0 \frac{v}{c} \tag{2.7}$$

where g is the gravitational constant of acceleration, f_0 is the operating frequency of the radar, c is the vacuum speed of electromagnetic waves and v represents the component of the surface layer water velocity parallel to the direction of the radar beam. In Figure 2.3 presented by Heron and Prytz (2003), the recorded back-scatter spectrum reveals two first-order spectral peaks, positively and negatively Doppler shifted from the radar frequency. Positively and negatively shifted spectral lines are observed due to scattering from waves propagating toward and away from the observing radar. An additional offset due to the surface current component, Δf *(df)* is seen to deflect the spectral peaks from the theoretical Doppler shift due to Bragg waves alone (positions of the dashed lines).

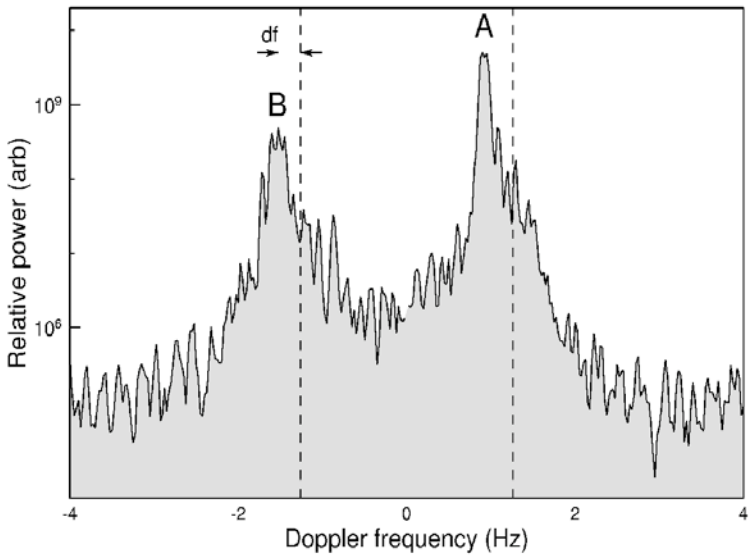

Figure 2.3 - Typical Spectrum for the VHF COSRAD Radar, Heron and Prytz (2003)

Range

In common with all radar operations, the scattering source or portion of ocean is identified by determining its azimuth (or direction) and distance from the observing station. Two main techniques exist among commercial coastal radar systems for determining the position of this target cell. Common to both techniques is the use of the properties of electromagnetic propagation speed to determine the range to target.

Range to target cell is essentially determined using the knowledge of the phase velocity of the transmitted electromagnetic waves. It is simply characterised by the equation :-

$$Range = \frac{c\ t}{2} \tag{2.8}$$

Where *c* is the velocity of electromagnetic waves and *t* is the propagation delay from the time of transmission to the time of reception.

The first ocean radar system to enter commercial use, the CODAR (Coastal Ocean Dynamics Application Radar) was originally developed at the National Oceanic and Atmospheric Administration (NOAA) by a team led by Barrick (1977). Of simple design, this system transmitted 20 µs long radar pulses and simply determined the range to target cell by time gating the received signals.

The range resolution of this system is proportional to the duration of the transmitted pulse. The disadvantages of this technique are the high peak transmission power required and a blind range in front of the radar related to the length of the transmitted bursts (Gurgel, 1999a).

A continuously transmitting radar system such as the Wellen Radar (WERA) described by Gurgel (1999a) uses a frequency modulated transmitted signal to determine the range to target cell. As described by Gurgel (1999a), Frequency Modulated Continuous Wave (FMCW) systems of this kind vary the transmitted frequency linearly over a period T, and use this transmitted sweep (or chirp) to phase coherently demodulate the returned radar echos. The range resolution of the radar is determined by the bandwidth, *b* of the frequency chirp over the time period, *T*. As shown by Gurgel (1999a), where the resolution of frequency is Δf, the range resolution is determined thus :-

$$\Delta\tau = \frac{T\Delta f}{b} = \frac{1}{b}\ , \quad \Delta r = \frac{c}{2}\Delta\tau = \frac{c}{2b} \qquad (2.9)$$

Because of this, these systems have the ability to select a desired range resolution by varying the bandwidth of the chirp. Other advantages of the FMCW systems are that they are more robust against radio interference (Gurgel, 1999b) and that there is no blind range in front of the radar. They do however require that the transmitter and receiver possess extremely high dynamic range and linearity, and also require that the transmit and receive antennae be placed to minimise coupling between them.

Direction

As with the determination of range to the cell, two different methods exist for determining the azimuth (direction) of the target cell. These are, direction finding techniques and beam forming techniques.

The original CODAR system (Barrick, 1977) and its commercial successor, the Seasonde as evaluated by Emery (2004), both use direction finding techniques to determine the azimuth to the target. The CODAR system developed by Barrick, initially used a phase direction finding technique using signals obtained from a linear three element antenna array. This was later modified to a four

element configuration (arranged in a square) to enable the determination of azimuth from all directions.

The Seasonde system uses the directional characteristics of a pair of crossed loop antennas (representing the x and y axis) and a monopole antenna (for normalisation of the loops) together with the MUSIC (Multiple Signal Classification) direction finding algorithm to locate the angular origin of received signals. As reported by Emery (2004) this is a relatively robust system. However, gaps can appear in the coverage which may result from the direction finding technique by the MUSIC algorithm. This is most likely because the technique or algorithm is unable to resolve more than two signals, at all times within a given range anulus. The main advantage of the Seasonde system is the small physical space required for the placement of its antennas.

As used by the WERA system (Gurgel, 1999a), beam-forming techniques produce a relatively narrow, steerable radar beam from a linear array of antennae arranged broadside to the region under investigation. The process of beam-forming is achieved in the time domain by summing the weighted and phase shifted signals from each antenna. Weighting reduces the side-lobes of the antenna array whereas the beam is steered through phase shifting. A WERA system operating in the High-Frequency Band will typically use 16 antennae in an array, with optimum spacing between individual antennae of a little less than half the radar wavelength (0.45 λ). This will achieve a beamwidth of approximately λ/D radians where λ is the radar wavelength and D is the overall length of the array.

2.3.2 Advantages, Limitations and Sources of Error

The ability of Ocean Surface Radar systems to provide high resolution spatial and temporal measurements over a wide surface area is seen to be their greatest advantage over single point current meters. These systems make it possible to obtain finely detailed information about the structure of surface currents, making it possible to identify eddies and fronts (Lane, 1999). These structures cannot be measured with the same time resolution by any other

means. The radar systems are also safer to deploy than moored current meters, especially in areas where it may be hazardous to lay moorings or in channels with heavy ship traffic. Their deployment also does not require the use of an expensive research vessel. Other advantages are that they can be remotely monitored or provide real-time data via communication links, and that they are not generally affected by poor weather or high sea conditions.

The limitation of usable range is dependant on the amount of attenuation between transmission, reflection and return of the propagating radio wave (Gurgel, 1999b). The amount of signal attenuation and the amount of signal reflection from scatterers determines the level of signal return achieved. This, coupled with the effects of atmospheric noise and other external short-range and long-range radio interference determine the Signal-to-Noise Ratio (SNR) of the system. This Signal-to-Noise Ratio is a primary indicator in determining the usable range of the system and the amount of error. As presented by Gurgel (1999b) on the physical limitations of HF radar systems, the attenuation of the propagating radar wave depends on frequency, the salinity of the sea surface, sea surface roughness and distance. Higher frequencies are attenuated more than lower frequencies. Lower salinity also leads to higher attenuation. Since interference is more prevalent while using lower HF frequencies, a trade-off is often involved in choosing an operating frequency to carefully maximise SNR and therefore range, Barrick (1977). Similarly, the amount of returned echo is dependant on the presence of significant scattering waves having a wavelength of half the radar. Barrick (1977) selected frequencies within a range of 25 MHz to 26 MHz as these were rarely affected by ionospherically propagated interference and were back-scattered from often present ocean waves of wavelength, 6 m. Gurgel (1999b) states that although VHF frequencies are highly attenuated and possess very limited working ranges, they are not affected by interference from long-range radio sources, only local sources. Working with a radar frequency of 152.2 MHz, Heron and Prytz (2003) have successfully used a VHF radar system to obtain high spatial resolution (100 m) current maps to a limited range of 1.5 km. This has proven highly successful in the investigation of near shore ocean surface currents.

Signal-to-Noise Ratio is also affected by sea state (Paduan, 1996) and is reportedly related to the accuracy of measurements where it causes spectral line broadening (Graber, 1997). The addition of noise and the broadening of the spectral line has been seen in some systems to make it difficult to determine the centre of the spectral peak (Graber, 1997). The study in obtaining current measurements in a surf break zone using a VHF Radar by Heron and Prytz (2003) determined that although the location of the spectral peak may be degraded by line-broadening, it was still possible to accurately determine the spectral peak and its frequency under these conditions. Subsequently, the broadening of peaks did not significantly affect the ability of the VHF system to measure surface currents in these conditions.

Other errors may exist as a result of beam forming misalignment, spatial inaccuracies and the contamination from side-lobes (Fernandez, 1996).

Further limitations in the use of HF / VHF Ocean Radar systems are related to the physical aspects of deploying the observing stations. Particularly with HF WERA Systems, the siting of large antenna arrays can be limiting in the choice of deployment sites. Other factors to consider for all radar systems is the supply of power and communications requirements for the deployment site, and the licensing and allocation of operating frequencies and bandwidth.

2.3.3 Obtainable Measurements and their Characteristics

As already described, the main product obtained from an Ocean Surface Radar is a high-resolution vector map of surface current velocities for areas of the ocean surface. The Ocean Surface Radar is unique in this regard. Although well designed surface drifters can be used to accurately measure surface currents they are very limited in their space scales and time-scale sampling (Paduan, 1996). Throughout the development of the Ocean Radar there have been numerous comparisons of HF Radar measurements with established single point methods of current measurements, such as those performed by Teague (2001), Graber (1997), Stewart and Joy (1974) and Barrick (1977). Graber (1997) specifically identifies a single point measurement as representing

a fixed-length temporal average at a point, while a radar observation represents a short-duration spatial average of a fixed area.

The radar measurements observed at the centre of an observation cell are in fact spatially averaged current measurements for this cell. This is due to the back-scatter and therefore Doppler shift resulting from the average surface current within the entire range cell. Variability of the measurements obtained can also be reduced by averaging over longer time periods (Emery, 2004). Another aspect of the measurements obtained is that they represent a weighted average over a depth from the surface. As investigated by Stewart and Joy (1974), this depth is dependent upon the radar frequency used. The scattering ocean waves corresponding to the radar wavelength are affected by a current to a depth proportional to their wavelength. Assuming a linear current profile near the surface, it has been defined thus :-

$$\text{Effective Depth} = \frac{\lambda}{4\pi} = \frac{1}{2k} \qquad (2.10)$$

where λ is the radar wavelength and k is the radar wavenumber. This was found to be consistent with an experiment using Multifrequency Coastal Radar (MCR) by Teague (2001). However, better agreement was suggested in some situations using $\textit{Effective Depth} = 1.4\ (2k)^{-1}$. In this study by Teague (2001) and an earlier study by Vesecky and Teague et al. (1998) it was shown that multifrequency radar provided the ability to observe near-surface currents at varying depths. With the range of frequencies used, current measurements were obtained for effective depths of 0.5 m to 2.5 m, though these were insufficient to generate surface layer current velocity profiles. The combination of results from the Multifrequency Radar and ADCP measurements for bins 2 - 14 m below the surface did however provide a more complete evaluation of the vertical structure within the water column.

2.3.4 Application to a coastal inlet for the estimation of mass transport

Coastal Ocean Radar using HF Frequencies to map current velocities off coastal regions to distances of up to 80 km offshore has been well documented by various authors such as Paduan (1996), Fernandez (1996) and Barrick (1974). The use of these systems has also been used in investigating large scale coastal channels such as the North Channel between England and Ireland (Knight and Howarth, 1999). While the use of HF Coastal Ocean Radar is quite well developed, the application of this technology to small scale coastal inlets and channels of the order a few kilometres across is not well researched. To provide adequate range resolution for such an application, the use of VHF frequencies is required. Although such VHF frequencies are highly attenuated and subsequently systems have very limited ranges of only a few kilometres, this is sufficient to map the currents in ports and coastal inlets. As mentioned earlier, the COSRAD system used by Heron and Prytz (2003) provided a range resolution of 100 m over a limited range of 1.5 km. This system provided high spatial resolution current measurements for a near-shore region. According to the effective depth analysis of Stewart and Joy (1974), these results would have represented a depth weighted average measurement of the upper 15.7 cm of the water column.

Other important aspects of the deployment of Coastal Ocean Radars are the physical locations of the observing stations. With only a limited system range and a specific region of investigation, the positioning of the radar systems is critical to obtaining the required measurements. The Radar Observing Stations must be located to ensure that the angle of intersection of both radar station beams is at least 30˚ for the region of interest (Graber, 1997). Regions with any intersection angle less than 30˚ are generally discarded because the errors involved in computing vector current become unacceptable.

2.4 Measuring the complete velocity profile

2.4.1 The need for a combination of measurement systems

Each of the measurement technologies presented in the previous two sections have individual shortcomings in their ability to profile the entire cross-sectional area of a coastal inlet. An ADCP mounted on the sea bed is able to provide accurate velocity measurements throughout most of the vertical water column but only for a single geographical point. It also lacks the ability to accurately profile currents close to the surface. Conversely, an Ocean Current Surface Radar operating at a fixed frequency cannot provide current measurements for anything except the surface layer. It can, however, provide these measurements across a wide area to a high degree of accuracy and high spatial resolution. A combination of these two technologies will extend the measurements of water current velocities across an Inlet.

Both the Broadband ADCP and Ocean Radar current measurement technologies have developed to the point where they are accepted and valued as useful tools for coastal oceanographic purposes (Graber et al, 1997 and Rowsell, 2002). In many studies using both these tools, the combined use has been limited to verifying the data acquired by HF Radar systems (Teague, 2001; Lane, 1999 and Graber et al, 1997). Now that the Ocean Radar technology is established, its use in conjunction with ADCP data should be able to provide a more detailed analysis in applications of coastal oceanographic research.

2.4.2 Examples of the use of combined measurement strategies

There is a very limited number of research activities where both Acoustic Doppler Current Profilers and Ocean Surface Current Radars have been used in an integrated measurement approach. A single study of particular key interest was performed by Howarth et al. (1995) and Knight et al. (1999). This experiment referred to in both publications investigated the net flow through the North Channel between Scotland and Ireland using measurements obtained from both ADCPs and the Ocean Surface Current Radar (OSCR) HF Radar

system. The ADCP was mounted on the sea bed in a low-profile frame at position E as shown in Figure 2.4, whereas the two Ocean Radar observing stations were positioned at Portpatrick and Crammag Head. The 150 kHz, 20˚ ADCP was deployed on the sea bed at a depth of 142 m and provided current measurements from 12.5 m above the sea bed to within 15 m of the surface. The OSCR Radar system provided surface current measurements across the entire channel except for an area of measurements close to the Irish Coast, which were beyond the limit of the system's usable range. The data from this area were discarded due to poor signal return and interference. However, they were not considered vital in the calculation of mass transport due to the shallow depth in this region.

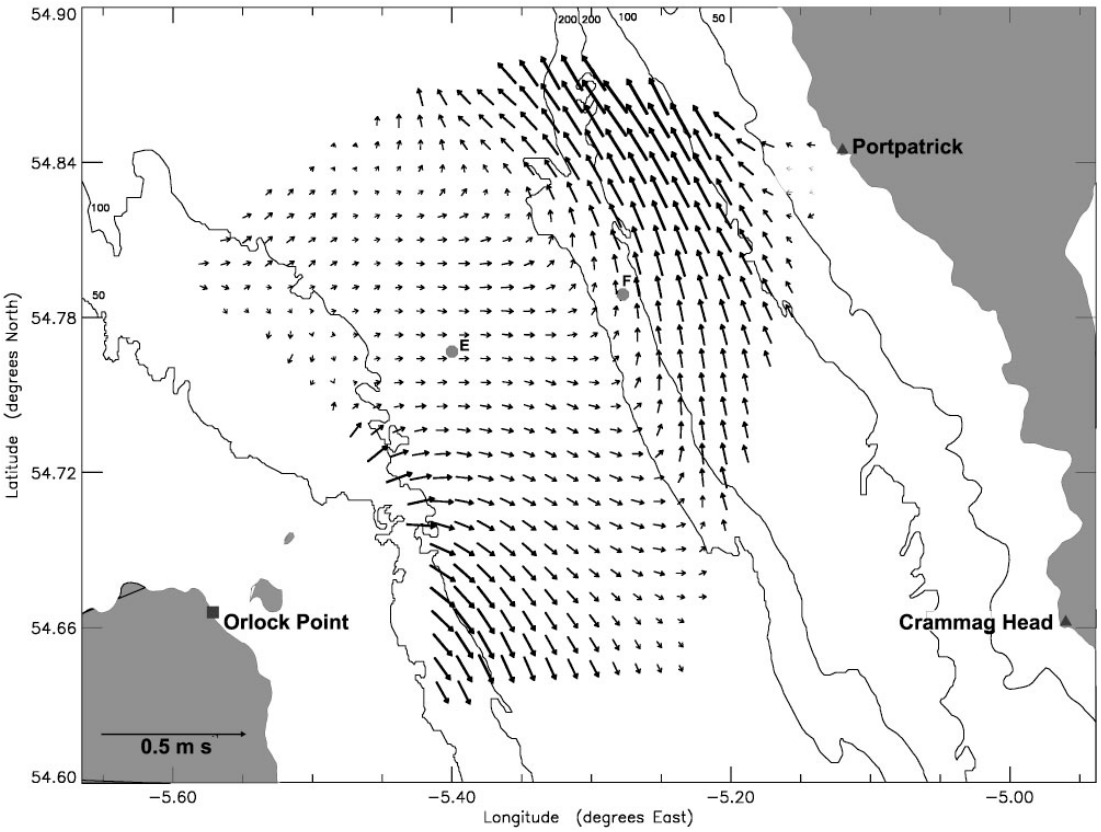

Figure 2.4 - Surface mean flows obtained from OSCR HF Radar
E - Seabed Mounted ADCP
F - S4 and RCM-7 Current meter mooring
▲ - OSCR Radar Stations
(Knight et al. ,1999)

The study of the North Channel focused on the residual flow caused by atmospheric pressure-systems and wind-stress on the ocean surface. Once the

tidal effects were removed, the analysis revealed quite complex residual flows. With the use of a simple residual current and wind stress correlation model it was suggested that large wind stresses were significant for residual flow. It was discovered that even on daily time scales, wind stresses could induce southward flows as well as northward flows within the channel.

A strong variation in the surface current was observed across the channel with complex flows present on the western side of the channel and strong currents close to the Scottish Coast directed towards the North-West. The ADCP data also showed complex current patterns within the vertical structure. At the ADCP Point E, a mean current near the sea bed was directed North-Westerly out of the Irish Sea while near the surface the current was directed into the Irish Sea.

Through the combined use of ADCPs and Ocean Radar systems, this study was able to provide a detailed investigation into the complex effects of wind stress on residual currents. In particular, this provided the means to estimate the mass transport taking into account both the horizontal and vertical variations of the current flow through the channel. The use of a single measurement technology alone would not have revealed the complexity of these currents in the North Channel.

2.5 Conclusion

The estimation of mass transport relies on successfully obtaining current measurements throughout the entire cross-sectional area of the flow, or transect of investigation. Measurements of both surface current and currents throughout a depth of water are not possible using one measurement tool alone. It has been shown that Acoustic Doppler Current Profilers provide accurate current flow measurements throughout the vertical column of water at a single point. This is useful in deriving vertical velocity distribution profiles near to the sea bed. Due to the inability of a sea bed mounted ADCP to profile currents in the surface layer plus its limitation to a single geographical point, an additional instrument such as an Ocean Surface Current Radar is required to provide surface current measurements.

Although the combined use of ADCPs and HF Ocean Radar systems has previously been used to determine mass transport through the North Channel between Ireland and Scotland by Howarth and Knight et al. (1995 and 1999), generally this technique remains undeveloped. To date there have been no publications regarding the use of both ADCPs and VHF Ocean Radars to evaluate mass transport through shallow coastal inlets. It is apparent that this area of knowledge would be significantly added to by a study involving the deployment of Acoustic Doppler Current Profilers and a VHF Ocean Radar system to evaluate mass transport and residual currents.

3 Research Design

3.1 Introduction

An experiment was proposed to accurately measure current velocities through a shallow coastal inlet using a current measuring scheme similar to those discussed in the previous chapter. An Acoustic Doppler Current Profiler was used together with the PortMap Surface Current Radar operating in the VHF band. It is expected that the combination of data from these two technologies would provide the most comprehensive means for estimating mass transport through the channel.

This research was conducted as part of an international project involving a partnership between James Cook University, Queensland Science and Engineering Consultants Pty. Ltd. (QSEC), and a greater consortium consisting of the Italian Organisations, the Italian National Institute of Oceanography and Applied Geophysics (OGS - Trieste), the Italian Institute of Marine Science (CNR-ISMAR - Venice) and the Consortium for Co-ordination of Research Activities concerning the Venice Lagoon System (CORILA). The main purpose of this collaborative project was to deploy the PortMap VHF Radar system to observe the surface currents in the Lido Channel entrance to the Venice Lagoon. This surface current data is to supplement the data from existing instruments already deployed to observe the current dynamics within the Lido channel. This will complement research already being undertaken by the Italian organisations regarding marine coastal circulation and water exchanges between the Venice Lagoon and the open sea. The combination of these data will provide detail of the surface current structure that is not possible with the existing instrumentation. The various sources of data and their contributors for the project are presented in Table 3.1.

Instrument	Contributor
Seabed ADCP - Lido Channel	OGS - Trieste, Italy
Tide Gauge - Lido	CNR-ISMAR - Venice, Italy
Meteorology Station Data	CNR-ISMAR - Venice, Italy
PortMap VHF Radar System	JCU / QSEC - Townsville, Australia

Table 3.1 Data Sources and Contributors

The next section will describe the chosen experimental site and surrounding environment. Following this, an overview of the various scientific instruments provided by the Italian organisations will be described. The VHF PortMap Radar and its deployment is detailed separately in the following chapter.

3.2 Experiment Location

Surrounding the City of Venice in Italy is the Venice Lagoon. This is the largest lagoon in the region of the Adriatic Sea, having a surface area of 550 km^2.

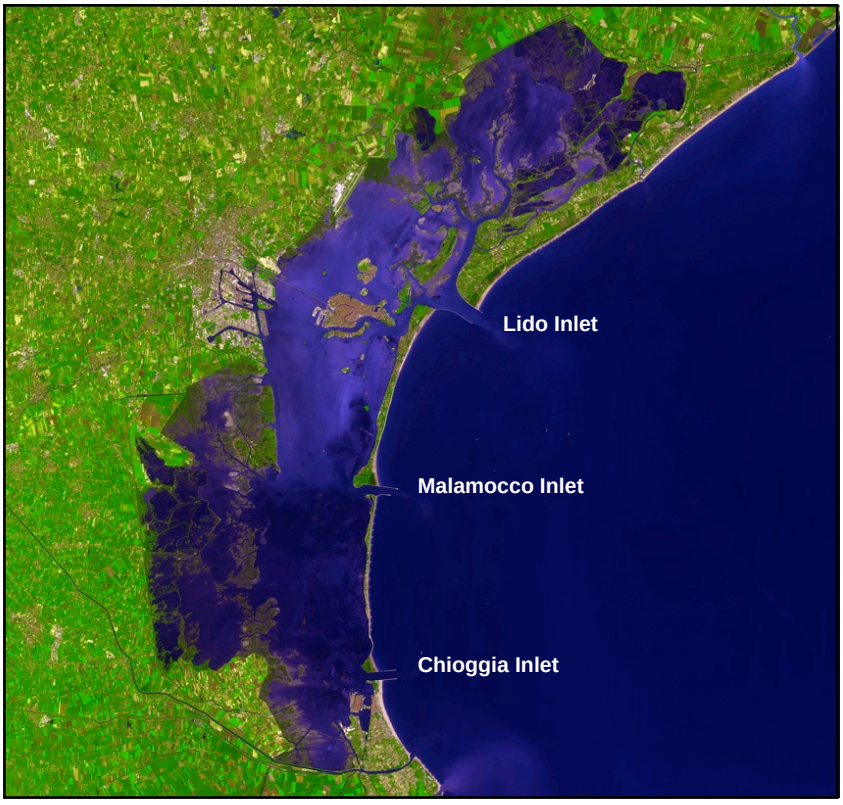

Figure 3.1 - The Venice Lagoon
(Image courtesy of Nasa Earth Observatory)

The Venice Lagoon is mostly quite shallow consisting of 80% mud flats and salt marshes and having an average depth of only 0.5 m. Three inlets connect the lagoon to the Adriatic Sea. These are the Lido Inlet, the Malamocco Inlet and the Chioggia Inlet (Figure 3.1). The Lido Inlet is situated in the Northern section of the Lagoon, the Malamocco Inlet is a little further south of this and the Chioggia Inlet lies at the southern most end of the Lagoon.

The Lido Inlet is a shallow, tidal inlet having a maximum width of 900 m across, an average depth of approximately 12 m and a typical tidal range of between 0.3 m - 1 m. As can be seen in Figures 3.1 and 3.2, Venice is the largest island in the centre of the Lagoon, with the Lido Channel closely situated directly to the east. The peninsula directly north of the Lido channel is called Punta Sabbioni whereas the narrow island to the south is known as the Lido.

Figure 3.2 - Venice and the Lido Channel
(Image courtesy of Nasa Earth Observatory)

Artificial breakwaters constructed of rock, concrete and concrete tetrapods extend out into the Adriatic Sea from both the Punta Sabbioni and the Lido sides of the channel. Lighthouses have been constructed at the end of these breakwaters to aid shipping navigation. The Lido channel is navigable by shipping and is the primary entrance used by Cruise Liners and Passenger and

Car Ferries to gain access to the Port of Venice. A network of deep shipping channels and smaller canals have been dredged and maintained throughout the lagoon to facilitate access for shipping. The mainland Commercial Port, located on the western side of the Lagoon at Marghera is accessed via the Malamocco Inlet to the south.

The investigation of mass transport and small-scale dynamics through the Lido Inlet is of particular interest due the occurrence of flooding events which affect the City of Venice. These floods known locally as “acque alte” (High Waters) are caused by the combination of astronomical high tides and various meteorological conditions. The meteorological effects can include a combination of heavy rainfall, periods of strong winds from the Bora or Sirocco winds and the presence of low pressure weather systems. These flooding events cause significant damage to the historic architecture and present an economic and social cost to the city. To protect the city from these flooding events, the construction of a barrage gate system known as the “M.O.S.E. Project” has begun at all three inlets to the Venice Lagoon. M.O.S.E., standing for Modulo Sperimentale Elettromeccanico is a flood-gate system consisting of 79 hollow, hinged floodgates that are normally housed within the seabed. When a flooding event is predicted, the system is activated to protect the city. Compressed air is forced into each gate causing the expulsion of water and therefore making the floodgate buoyant with one end rising to the surface (Figure 3.3). Once deployed, these floodgates effectively separate the Lagoon from the Adriatic Sea thereby protecting the City of Venice from the

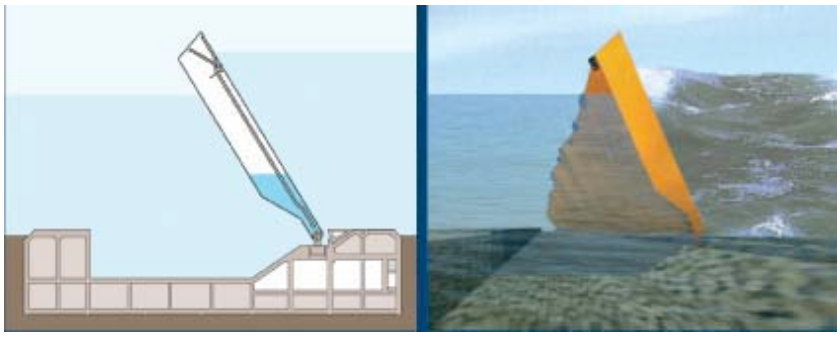

Figure 3.3 - M.O.S.E. Flood-gate deployed
(Image courtesy of Venice Water Authority)

damaging high waters. There has been much controversy surrounding the construction of the M.O.S.E. Project and concern exists about the effectiveness of this system and the impact that periodic closures of the inlet channels will have on the Lagoon environment. As such, particular importance has been placed on investigating the dynamics of the Venice Lagoon and its inlets by the Italian research organisations involved. Some of the previous studies conducted by these organisations have emphasised the investigation of water flow between the Venice Lagoon and the Adriatic Sea (Gacic, M. et al, 2004, 2005).

To complement this ongoing research, the Lido Inlet was selected as the most suitable inlet for the deployment of the PortMap Radar. The two stations of the radar system were set up at the lighthouses at the end of the Punta Sabbioni and Lido breakwaters. The lighthouse positions at each of the seawalls provided convenient access to a power source, security and protection from the elements for the electronic equipment. The geographical and physical positioning of the transmit and receive antennas was also optimal to provide radar coverage of the channel and surrounding sea areas. Furthermore, it was possible to obtain convenient access for monitoring the stations and collecting data files from the station computers during the deployment.

3.3 Deployment Period

The deployment of the PortMap VHF Radar system at the Lido Inlet was undertaken from the 1st October, 2005 until the 11th November, 2005. This would provide continuous data of the surface currents within the channel and outside of the channel for a total duration of 6 weeks. As “acque alte” flooding events in Venice commonly occur during the months of October and November, it was expected that the observation period would encompass a flooding event.

3.4 Acoustic Doppler Current Profiler

To provide subsurface measurements of the current through the channel, an upward looking Acoustic Doppler Current Profiler (ADCP) was deployed on the sea floor within the Lido Channel entrance to the Venice Lagoon. Other similar instruments were also placed in the Malamocco and Chioggia Inlets. These instruments were successfully used in previous studies to record current flow measurements in the channels between the Venetian Lagoon and the open sea (Gacic et al., 2004).

The placement of the ADCP in the channel was determined by Gacic et al. (2004) in previous studies. A process was undertaken for positioning the single ADCP in the channel where the measurements obtained would be most representative of the total water flux through the channel. Initially, current profiles for a channel transect were obtained using a ship-borne ADCP. On average, 100 transect profiles were taken at each inlet, at various phases of flood, ebb and slack tides. From the profiles, the water flux through each inlet was obtained using the proprietary ADCP post-processing software, WinRiver by RD Instruments. Using a linear regression calculation, the resultant value for water flux at various states of the tide was compared to corresponding vertically averaged currents for various points across the transect. The selected location for the ADCP was at a point on the transect where the linear correlation between these was a maximum, thereby making the single point location measurements indicative of the inlet water transport rate.

The chosen location for the ADCP in the Lido Inlet is at position 45°25'21.00"N, 12°25'35.60"E as shown in Figure 3.4. This position is closest to the Lido side of the channel and within the deepest portion of the channel. Mounted on the sea floor, the self-contained ADCP requires regular inspections by CNR-ISMAR staff to retrieve data and for maintenance and cleaning. The ADCP continuously acquired data during the six weeks of the PortMap Radar deployment, except for a short duration on the 12th October when it was retrieved for data collection and maintenance. As can also be seen in Figure

3.4, the location of the ADCP is within the estimated range of the PortMap Radar system.

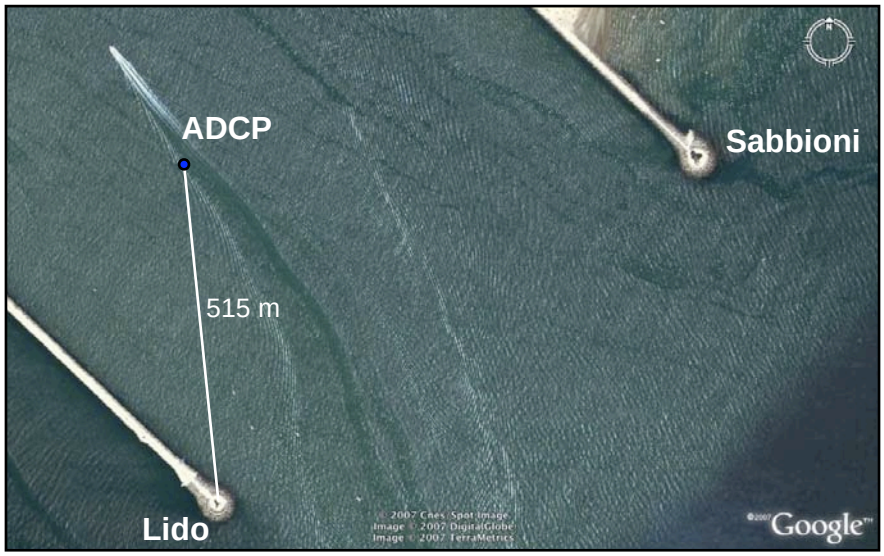

Figure 3.4 - ADCP Location, Lido Channel
(Image map courtesy of Cnes/Spot, DigitalGlobe, TerraMetrics and GoogleEarth)

The ADCP used in the Lido channel is an RD Instruments Workhorse Sentinel operating with an acoustic frequency of 600 kHz. It has been set at a vertical profiling resolution of 1 m depth cell size. At this operating frequency and depth cell size, the Workhorse Sentinel model is capable of a maximum range of 43 m which is more than adequate for its deployment in this channel which is no more than 14 m deep. Current speed and direction are recorded onto an internal memory card every 10 minutes as an average of 60 pings. The Workhorse Sentinel ADCP features four transducer beams with 20˚ beam angles. In its position on the sea floor at a depth of 13 m, the ADCP will theoretically only experience sidelobe interference within the upper 0.78 m of the water column, based on the formula given in Section 2.2. The four transducer design provides good data reliability with a redundant data source for resolving three dimensional current velocities. In the case of a blocked beam or failure of one of the transducers, current measurements are still obtained with the remaining three transducers. With all four transducers operational, however, an error velocity measurement is provided that can be used to evaluate horizontal homogeneity within the flow and subsequently, the accuracy of the measurements obtained.

3.5 Additional Instrumentation

Through the Italian partners to the project, additional data from tide gauges and meteorological instruments have been made available for the duration that the PortMap Radar was deployed.

Tide data from stations at the Lido, Malamocco and Chioggia Inlets have been provided. Additional data have been provided from a station at Punta della Salute in the City of Venice, and a tide gauge at the oceanographic tower situated approximately 7 NM SSE of the Lido Lighthouse. Tide level data from all these tide stations have been recorded at 5 minute intervals.
A Meteorology station, also situated on the oceanographic tower has provided the measurement of :-

- atmospheric pressure
- air temperature
- water temperature
- relative humidity
- solar insolation
- average windspeed
- maximum windspeed
- average wind direction
- rainfall

The anemometer used to record wind speed and direction measurements is at a height of 15 m above the average sea level. All the meteorological data have also been recorded at 5 minute intervals. These data sources will be sufficient to validate and to supplement the data provided by the PortMap Ocean Surface Current Radar.

4 PortMap Radar and Deployment

This chapter presents a brief overview of the historical development of the PortMap radar, followed by a detailed description of its range and azimuth resolving methods, hardware design, and data acquisition and control software. Also covered are the test deployments undertaken in Townsville and the deployment of the system to measure surface currents within the Lido Inlet, Venice.

4.1 Development of the PortMap Radar

The Portmap Ocean Surface Current Radar (PortMap) is a further development on the well published James Cook University's COSRAD system referred to in Chapter 2 (Heron and Prytz, 2003). The COSRAD system is a pulsed Ocean Surface Current Radar similar to the original CODAR system presented in the first chapter, however it operates in the VHF band. This system has been successfully used to investigate fine-scale structure in surface flow for a number of coastal settings and experiments. These include deployments to investigate the interaction of tidal flow from the Barra Nova Inlet in Ria Formosa (Portugal), the mapping of coastal currents for the placement of Coffs Harbour sewage outfalls, and measurements for coastal engineering planning for Cairns Port Authority and Geraldton Harbour board. An example of the current mapping capability for the Coffs Harbour deployment is depicted by the current map shown in Figure 4.1.

This system was capable of producing surface current maps with a range resolution of 100 m up to a range of 1.5 km. The system used a steerable, rotating pedestal with a 4-element linear antenna array that was used for both transmission and reception. It achieved this by transmitting 670 ns long radio wave pulses on a frequency of 152.2 MHz through the antenna array. These pulses were spaced 2 ms apart. Since this system spends the majority of the transmit/receive duty cycle in receive mode, its overall range was limited by the high peak power required within the short transmit time. A further limitation is

the blind range in front of the radar that is not observable because the system is still transmitting while return signals would be observed from the near range. For a 670 ns pulse, this corresponds to a blind range of 201 m in front of the radar with an additional distance to allow for transients in the Transmit/Receive switch to settle down.

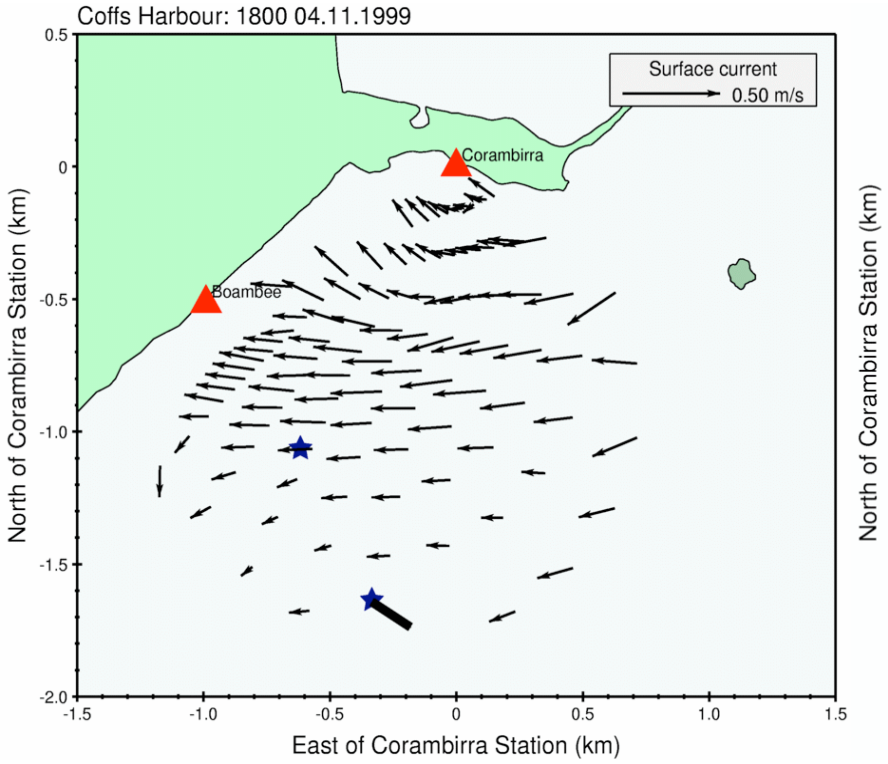

Figure 4.1 - COSRAD Current Map (Heron and Prytz, 2003)

The PortMap radar, produced by a group led by Helzel Messtechnik GmbH is aimed at overcoming some of the limitations inherent in the COSRAD system. The technology of the established WERA HF Ocean Surface Current Radar has been adapted to operate in the VHF band to provide short-range, high spatial resolution measurements. As such, both PortMap and WERA are continuously transmitting, chirped frequency-modulated continuous wave (FMCW) radars. The primary advantage of using a continuously transmitting scheme over the existing COSRAD pulsed system is that a greater maximum operating range should be achievable with a lower peak output power required. This will be with the same 100 m spatial resolution as the COSRAD system. Similar to the COSRAD system, the PortMap radar uses a steerable, pedestal mounted

receive antenna array, but with a separate transmit antenna mounted on a central pole. The PortMap system retains the advantages of the COSRAD system in being easily deployable with a compact antenna system.

4.2 PortMap Radar, Frequency Modulated Continuous Wave Operation

The PortMap radar uses linear FMCW chirps to continuously transmit and receive radio wave signals to and from the ocean surface under investigation. The details of the operation of this continuously transmitting FMCW system presented here for the PortMap radar are as outlined by Gurgel (1999b) for the Wellen Radar (WERA).

4.2.1 Range Determination

As with all radar systems, range determination is derived as a function of the propagation time delay between transmission and reception and the speed of light, as presented in Chapter 2 by Equation 2.8.

As time gating cannot be used in a continuously transmitting system to determine range to target cell, another technique is used. The PortMap system transmits linear frequency chirps as represented by

$$s(t) = \sin \left[2\pi \left(f_o + \frac{b}{2T} t \right) t \right] \qquad (4.1)$$

where the frequency of the transmitted signal varies linearly from f_o to $f_o + b$ over the chirp period, T. The system repeats the transmission of this signal. Continuing with the analysis presented by Gurgel (1999b), the received signal is comprised of the superposition of HF waves backscattered from all ranges, as

represented by

$$r(t) = \int \alpha\ (\tau)\ \sin\ [2\pi\ (f_o + \frac{b}{2T}(t-\tau)\ (t-\tau)\ + \phi]\ d\tau \quad (4.2)$$

where τ is the propagation time between transmission, scattering and receiving. The amplitude $\alpha(\tau)$ and phase $\varphi(\tau)$ vary with time due to the scattering surface waves (assumed to be constant during chirp period, *T)*. After phase-coherent demodulation, the received signal is comprised of the in-phase and quadrature time series representation

$$z(t) = \int \frac{\alpha\ (\tau)}{2}\ exp\ \left[i\left(-2\pi\frac{b\tau}{T}t + \phi(\tau) + \varphi(\tau)\right)\right]\ d\tau \quad (4.3)$$

Resolving this signal into ranges is achieved from the Fourier transform of each single chirp. From this, the resolution of the frequency f = *b* τ / *T* , is determined by the length *T* of the chirp, i.e. Δf= 1 / *T*. This therefore dictates the resolution of both propagation time and range resolution as

$$\Delta\tau = \frac{T\Delta f}{b} = \frac{1}{b}\ , \quad \Delta r = \frac{c}{2}\Delta\tau = \frac{c}{2b} \quad (4.4)$$

Using this relation, the Portmap Radar operating with a bandwidth, *b* of 1.5 MHz and speed of light, *c* has a range resolution of 100 m.

The next step is the Fourier transformation of each chirp. This must be implemented with a windowing function to prevent any leakage problems associated with the spectral analysis (Gurgel, 1999b). This leakage can cause high energy signals from near ranges to mask low energy signals from more distant range cells. After the application of the Fourier transform to each chirp, the resulting amplitudes represent the slowly varying modulation of the backscattered signal from the scattering surface waves.

Once sorted into range cells, this result becomes

$$v(n\Delta r, t) = \alpha(n\Delta\tau, t)\, \exp\left[i\, \varphi(n\Delta\tau, t)\right] \quad (4.5)$$

where n is the range cell number. The resulting time series data for the sample period is equivalent to the results achieved with a pulsed radar such as the COSRAD or CODAR systems, but with continuous transmission and reception. For each receiver (antenna element), the time series data collected for the various range cells is a superposition of all backscattered signals from all directions within that annular range cell.

4.2.2 Azimuth Determination

The PortMap radar uses a four element, linear antenna array for the receiving of signals. The signal from each antenna element signal is received and processed as above to provide Fourier transformed I and Q channel time-series data for each range cell. As amplitude and phase information is recorded for each channel, either beam forming or direction finding techniques can be used to determine the azimuth to the target area. This will be covered in further detail in section 4.4 Radar Antenna System, of this chapter.

4.3 Electronic Hardware and Operation

The PortMap system uses a combination of electronic hardware for the radio frequency sub-system and real-time embedded computers to perform the various control and processing tasks. These are all contained in a portable 6 unit 19” rack case, as shown in Figure 4.2. An additional workstation computer running the SuSE Linux operating system provides a user’s console for configuring and operating the system, and is also used for the storage of acquired data.

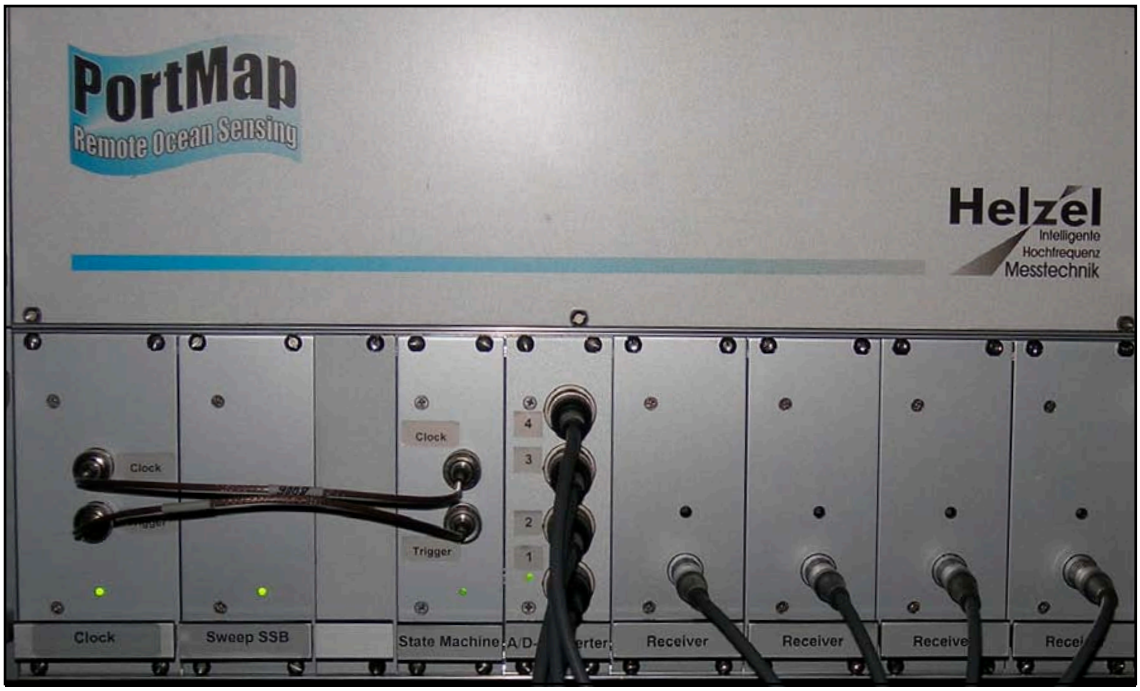

Figure 4.2 PortMap Rack Electronics

The most critical aspect of the operation of the FMCW design, is the linearity and phase stability of the generated chirps. This is achieved in PortMap by using a highly stable synthesiser as a master system clock. This system clock provides stable timing pulses for the State Machine and a Direct Digital Synthesiser (DDS) which are used for generating the FMCW linear chirps with low phase noise. The use of a DDS in the system provides an ideal method for generating linear chirps, with the added flexibility provided by software control. A block diagram of the hardware contained within the PortMap system is shown in Figure 4.3. The DDS generated chirp signal output by the Sweep Single Sideband (Sweep SSB) unit is split into five channels. The signal from one channel is used to drive the transmit amplifier where it is amplified to 16 dBm before feeding the transmit antenna.

Signals received at each of the receive array elements are bandpass filtered before passing to the receivers. The remaining four chirp channels are used by

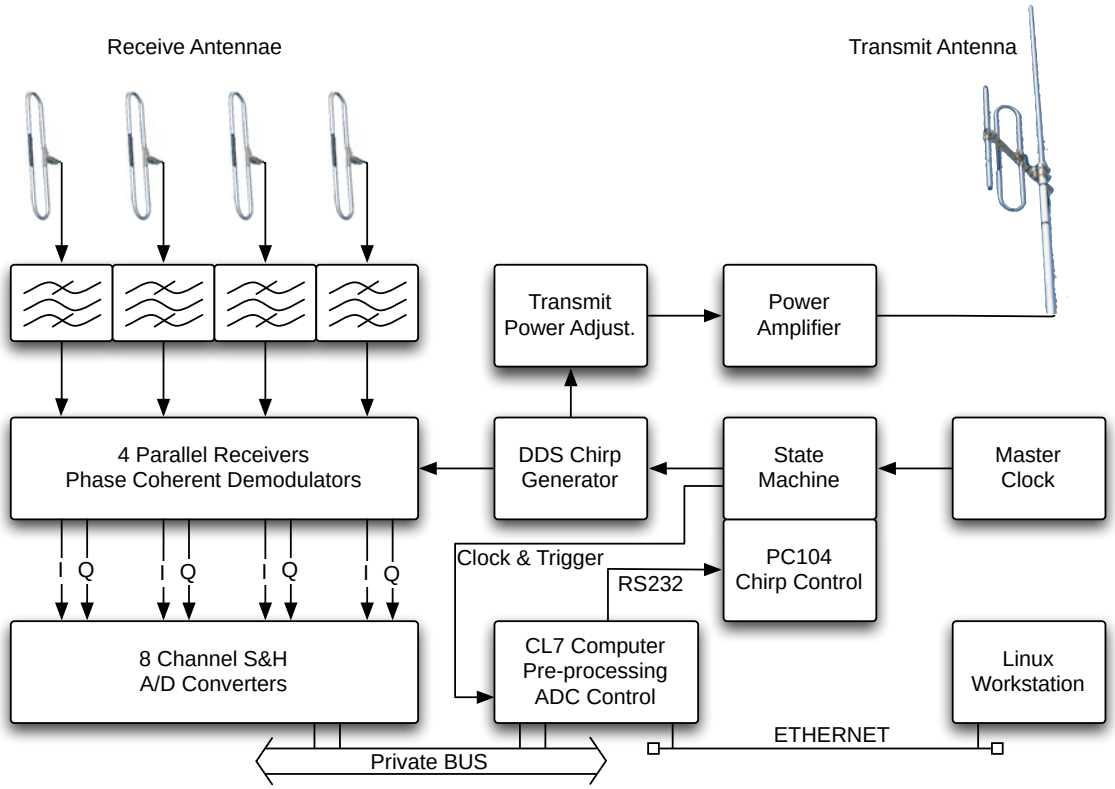

Figure 4.3 PortMap Hardware Block Diagram
(Adapted from WERA Diagram - Gurgel, 1999b)

the four direct-conversion receivers for phase-coherent demodulation. The demodulated I and Q channel signals are low pass filtered to prevent aliasing, before being sampled by the analog to digital converters (ADCs).

The ADCs are controlled by the CL7 Real-time computer. This unit receives commands from the Linux workstation at the commencement of a measurement run and initiates the chirp generation and the ADCs. Data acquired by the ADCs is buffered and transferred to the CL7 computer via a private bus. In real-time, the data are then resolved into ranges as per the FMCW range-resolving method using Fast Fourier Transforms. This range-resolved time-series of I and Q values is then stored in binary files on the Linux workstation by means of Network File Storage (NFS) protocols over the ethernet connection. The PC 104 computer also shown in Figure 4.3 is used to control the settings and sequences for the chirp generation. Parameters of these are configured on the Linux workstation and transferred via ethernet to the CL7 computer.

4.4 Radar Antenna System

The antenna system for the PortMap radar contains both transmitting and receiving elements in the same unit, along with motor control for the physical steering of the array. Physical steering of the array provides the ability to acquire data over a single sample period from one direction, before re-positioning the antenna to observe a different area of ocean. In addition to the physical steering, electronic steering is used to steer the receive array with +/-30˚ of the boresight direction. In this way, it is possible to cover a greater measurement area with more precise beam-forming or direction finding accuracy than would be possible with a fixed antenna. Even with this capability, the PortMap antenna system is designed to be lightweight, portable and easily deployed in the field.

Figure 4.4 PortMap Antenna System

Construction

The heavy steering motor and gearbox, and control unit are positioned at the base of the antenna to keep the centre of gravity low. To this motor base, a lightweight PVC housing is fixed. This housing shrouds the antenna cables and drive shaft and acts as a stable platform and bearing edge for the receive array bar. The receive array bar is fixed to a top cap which rests on this bearing edge. The drive shaft consists of shorter segments and is connected to the gearbox fitting, the top cap, and continues further up to the single transmit antenna mounted above. These three physical elements then rotate together under the control of the motor. The antenna cables within the PVC housing are allowed to move freely before exiting through the rotating top cap. The bar that the receive antenna array elements attach to is 3 m long corresponding to three half-wavelength (98.6 cm) sections which separate the four receive elements.

Unlike Ocean Radar systems operating at High Frequencies (HF), PortMap is operating in the Very High Frequency (VHF) band so the physical size of the antenna elements is quite compact. Small elements and the small cross section of structural elements help to limit the amount of wind-loading exhibited by the entire antenna. To keep the antenna stable, guy ropes are attached to the top of the PVC column and taken out to either fixed or temporary anchor points while the unit is deployed. As the unit is to be deployed in coastal areas where strong winds are likely, it is important that the structure is made secure.

Steering Control

The antenna rotation motor is controlled by a programmable logic controller (PLC) also housed within the motor base. This is remotely controlled from the PortMap workstation computer via an RS-232 or RS-485 communications link. The PortMap workstation computer sends an ASCII command string to move the antenna. This command string contains the integer value for the desired antenna angle (0˚ to 359˚ from start position). The PLC processes this command string and controls the motor such that the antenna only rotates +/- 270˚ from the start position. This is to prevent the cables inside the PVC housing from twisting too tightly.

On the PortMap workstation, a configuration file permits the user to define the desired antenna start position, the number of times to change, and the angle of change each time the antenna is rotated. A background program running on the workstation then advances the antenna to the next antenna angle in the sequence, one minute prior to data acquisition from that direction. The boresight angle of the antenna is recorded as meta-data in the acquisition file obtained for that direction.

Transmit Antenna

Since the receive antenna array elements are omnidirectional dipoles, the transmit antenna needs as high a front-to-back ratio as is possible. A Deep Null, 2-element Yagi antenna is used to achieve this on the PortMap system. According to the manufacturer's specifications, a nominal front-to-back ratio of 14 dB is achievable with a small forward gain of 6 dBi.

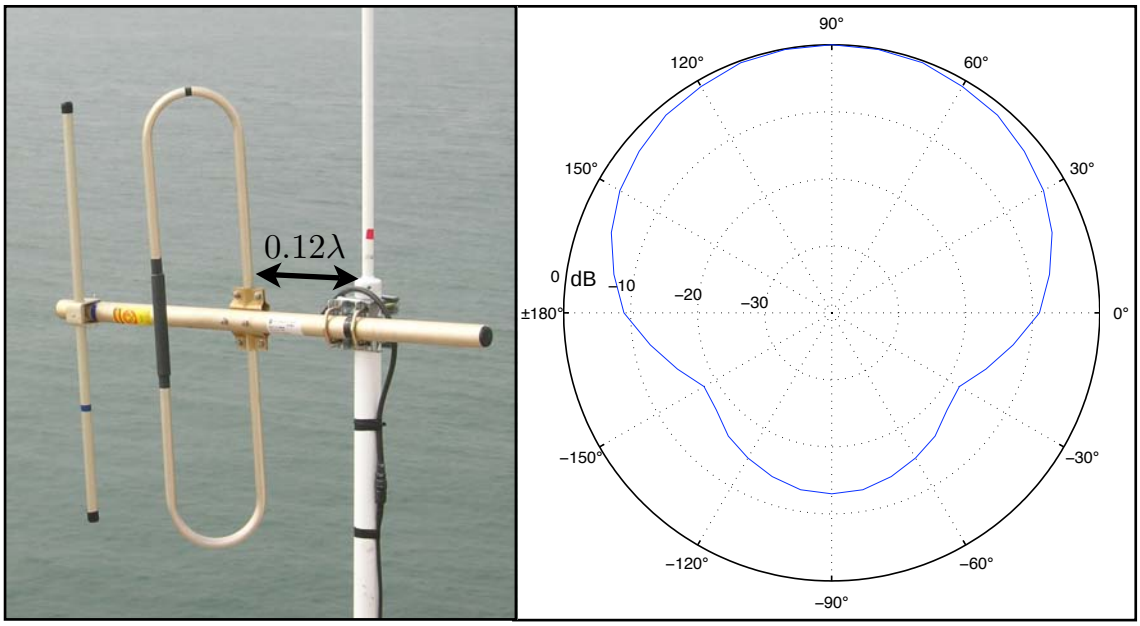

Figure 4.5 Deep Null Yagi Transmit Antenna and Polar Response

The Deep Null Yagi antenna achieves its very high front-to-back ratio by using the mounting structure (centre shaft) to act as a reflector for the antenna. This requires the mounting shaft to be spaced 0.12 wavelengths from the edge of the dipole (as shown in Figure 4.5). This distance is 23.7 cm for the operating frequency of 152.2 MHz.

Of particular note with this transmit antenna is the wide horizontal beamwidth of 130˚. As shown in the next section, this angle is significantly more than the beam forming acceptance angle of 60 degrees.

Specification	Value
Impedance	50 Ohm
VSWR	14 dB
Front / Back Ratio	14 dB
Horizontal Beamwidth	130˚
Vertical Beamwidth	70˚

Table 4.1 Transmit Antenna - Other Specifications

Phased Array Receiving Antenna

The azimuthal resolution of the PortMap system highly depends on the receive antenna array, and more specifically its beamformed radiation pattern and beamwidth. The receive antenna is a linear phased array of identical omnidirectional dipoles. The far field radiation pattern of this array is a direct result of the geometric arrangement, and the relative amplitudes and phases of the array elements, as well as the single element radiation pattern. This far field radiation pattern is because of the introduction of relative phase shifts in the radiation vectors, adding constructively in some directions while destructively in other directions. As our single element radiation pattern is isotropic, the array exhibits a radiation pattern dictated by the array pattern multiplication property where the total radiation vector is given by

$$\boldsymbol{F}_{tot}(\boldsymbol{k}) = A(\boldsymbol{k})\ \boldsymbol{F}(\boldsymbol{k}) \tag{4.6}$$

where ***F (k)*** is the factor due to a single element and

$$A(\boldsymbol{k}) = a_0 e^{j\boldsymbol{k}.\boldsymbol{d}_0} + a_1 e^{j\boldsymbol{k}.\boldsymbol{d}_1} + a_2 e^{j\boldsymbol{k}.\boldsymbol{d}_2} + \ldots \tag{4.7}$$

is the array factor.

Since $\boldsymbol{k} = k\,\hat{\mathbf{r}}$, the array factor may also be denoted as $A(\hat{\mathbf{r}})$ or $A(\theta, \phi)$.

For the 4-element PortMap array, the array factor can be written as

$$A(\phi) = a_0 + a_1 e^{jkd\cos\phi} + a_2 e^{2jkd\cos\phi} + a_3 e^{3jkd\cos\phi} \tag{4.8}$$

where *k* is the wave number, *d* is the antenna separation and ϕ is the steering angle. The PortMap array antenna dipoles are horizontally spaced along the array mounting bar with a half-wavelength separation distance of 98.5 cm. The operating wavelength is 1.97 m (*f* = 152.2 MHz). With this half-wavelength element spacing, unity amplitudes and no phase shift between the elements, the array pattern results in a directional beam broadside to the linear array, as shown in Figure 4.6. This pattern also shows that the linear array exhibits an equal response behind the array. This clearly shows the importance of the high front-to-back ratio of the transmit antenna presented in the section above. By constraining most of the transmitted power to the forward direction we are able to 'steer' the phased array through the radiated area to receive signals from the forward direction. The rear lobe is then not considered significant, as very little signal is received from this direction.

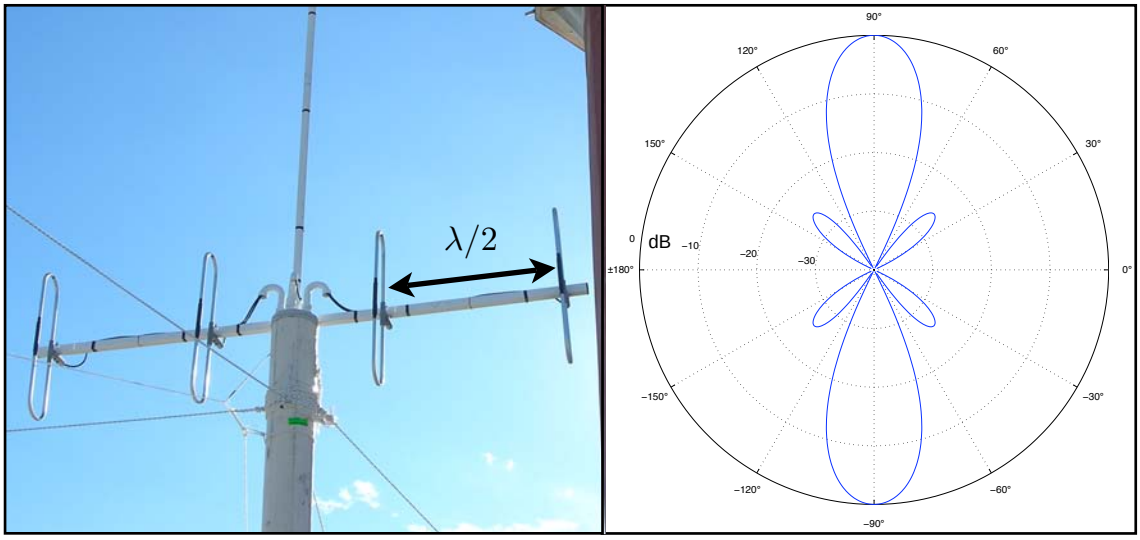

Figure 4.6 PortMap Receive Antenna Array and Polar Response

At this broadside steering position with no additional phase shift between the elements, we can evaluate the 3-dB beamwidth, $\Delta\phi_{3dB}$ by differentiating the equation $\psi = kd\cos\phi$, that is

$$d\psi = \frac{\partial\psi}{\partial\phi}d\phi = (-kd\sin\phi)d\phi \qquad (4.9).$$

If this derivative is evaluated at broadside (ϕ = 90˚) and assume a relatively narrow mainlobe, this becomes

$$\Delta\psi_{3dB} = \left|\frac{\partial\psi}{\partial\phi}\right| \Delta\phi_{3dB} = kd\ \Delta\phi_{3dB} \tag{4.10}$$

and solving for $\Delta\phi_{3dB}$, we obtain :-

$$\Delta\phi_{3dB} = 0.886\frac{\lambda}{Nd} \tag{4.11}$$

For the PortMap array, this calculates to a 3dB beamwidth of 25˚. This beamwidth applies only at broadside ϕ = 90˚. Beam steering is achieved by modifying the steering angle ϕ by introducing additional phase shift between the elements of the array. The pattern of the beam and the corresponding beamwidth varies as it is steered through various angles from ϕ = 0˚ to 90˚. This is seen in Figure 4.7 where additional phase shift between elements is incremented by $\pi/6$ radians for each subsequent polar plot.

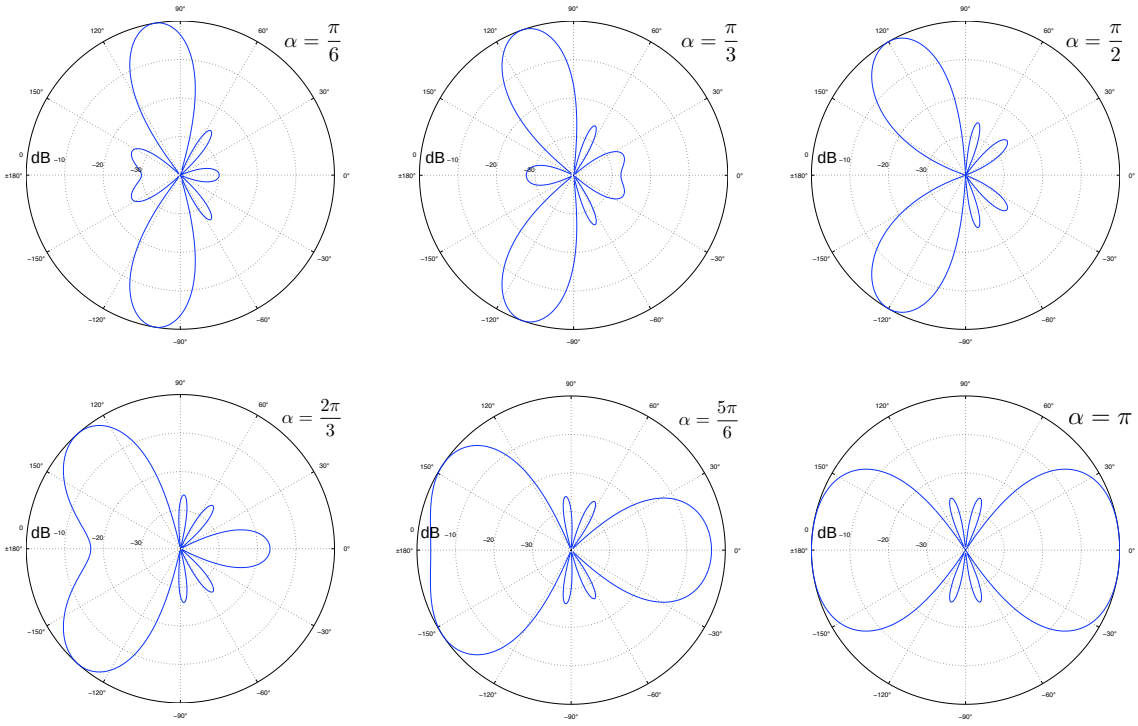

Figure 4.7 Steered Array Normalised Polar Plots (Element Phase Shift, α in radians)

The antenna pattern significantly broadens for angles, ϕ > 30˚ as seen in the last three subplots. Therefore, the practical physical limit that the beam can be steered with the phased array is +/-30˚ from the broadside direction. This corresponds to a phase angle, $\alpha < \pi/2$ radians.

In practice, the application of phase shift between the antenna elements is typically performed in the time domain. Since in the PortMap system each of the signals received by the individual elements are separately demodulated and have their I and Q time-series values recorded, this can be performed in software on either the time-series data or on Fourier transformed spectrum data.

4.5 PortMap Radar Control and Data Acquisition

User Control of the PortMap radar is via the Linux workstation running the SuSe Linux operating system. On this platform, a web based interface is used to control the radar parameters and timing of data acquisition. This interface communicates configuration settings to the other real-time computers in the system via the WeraDesk CGI binary. The real-time computers communicate back to the workstation by writing status information directly back to the workstation system drive, together with the acquisition data. The user interface for the PortMap workstation is shown in Figure 4.8 with the settings used for the Sabbioni Lighthouse deployment.

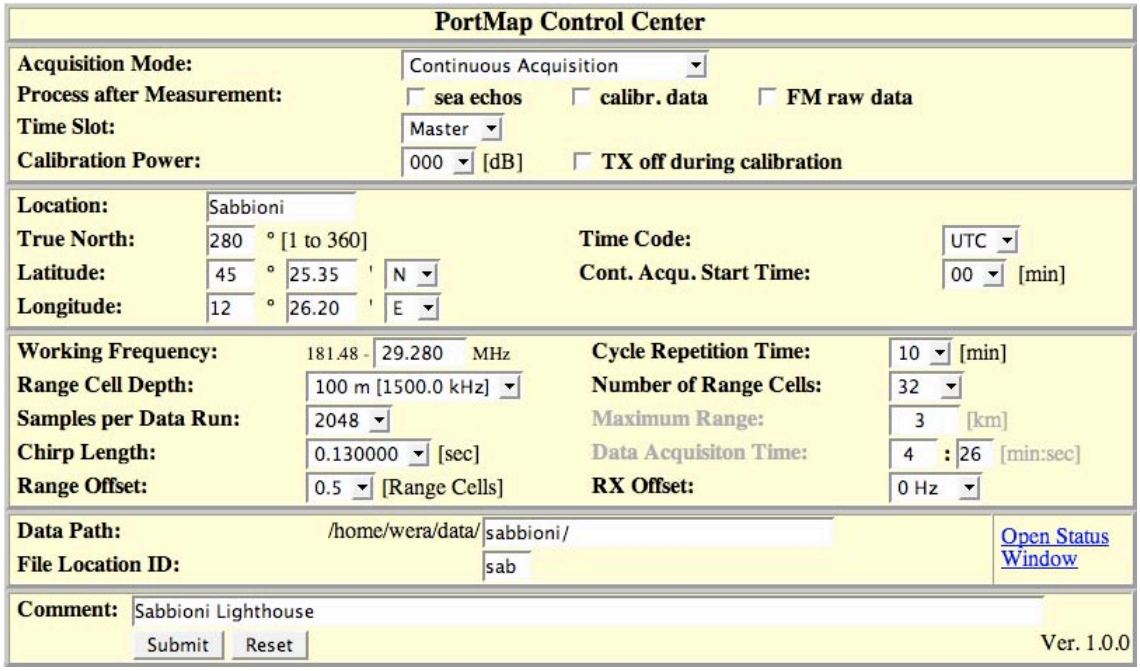

Figure 4.8 PortMap User Interface

Of particular note are the radar settings specified for working frequency, range cell depth, samples per data run, chirp length and number of range cells. These settings dictate the maximum range and the data acquisition time taken for the number of samples of a specified chirp length, i.e. 2048 x 0.13 Sec = 4 minutes, 26 seconds.

The data acquisition time determines the timing sequence that can be used, particularly with a Master and Slave, 2-station system. This is because both stations operate at the same centre frequency of 152.2 MHz. The Master Station takes 4 minutes, 26 seconds with a cycle repetition time of 10 minutes. This allows a Slave Station to start at 05 minutes and acquire data for 4 minutes, 26 seconds before the Master station repeats its acquisition. The real-time system clock on both station workstations provides the timing for both the antenna control and for the start of data acquisition. Because of this, it is important that the system clock is accurately set on both workstations, as there is no automatic synchronisation between the systems. Timing signals from the NAVSTAR Global Positioning System (GPS) could possibly be used to provide this level of synchronisation but are not presently used.

As described in Section 4.4, a separately modified configuration file, position.drv is used for controlling the antenna motion. A typical configuration file appears as :-

```
280  % Start Position in integer degrees
-60  % Position change in degrees (Negative - Anticlockwise)
-3   % Number of Position changes
280  % Current Position in Degrees (modified by software)
```

The fourth value in this configuration file is set by the antenna control program each time the antenna is rotated to a new position. This value is read by the PortMap Control Centre and displayed in the field “True North:” to indicate the boresight angle of the antenna. This value is also written as meta-data at the header of each acquisition file.

The range-resolved time-series of I and Q values that are stored as binary files on the workstation can be post-processed and analysed to produce additional data as required. This could be simply converting these binary time-series and storing them to an ASCII file, to the determination of current and wave measurements. For the PortMap system, post-processing software has been developed for Microsoft Windows as both a command-line tool (pmap2dat.exe) and as a graphical user interface (PortMap.exe) to perform these tasks on other workstations independent of the PortMap system. An example of the outputs available from the graphical user interface, PortMap.exe are shown on the next page. Figure 4.9 displays the I and Q channel time-series values for range cell 4, acquired from antenna #1. Figure 4.10 displays the power spectrum calculated from these values. This post-processing software could also be used to produce the beam-formed, time-series or power spectrum data for a particular azimuth angle within this range cell 4. This technique is the basis for obtaining data resolved in both range and azimuth, which will be covered in Chapter 5, Data Analysis and Results.

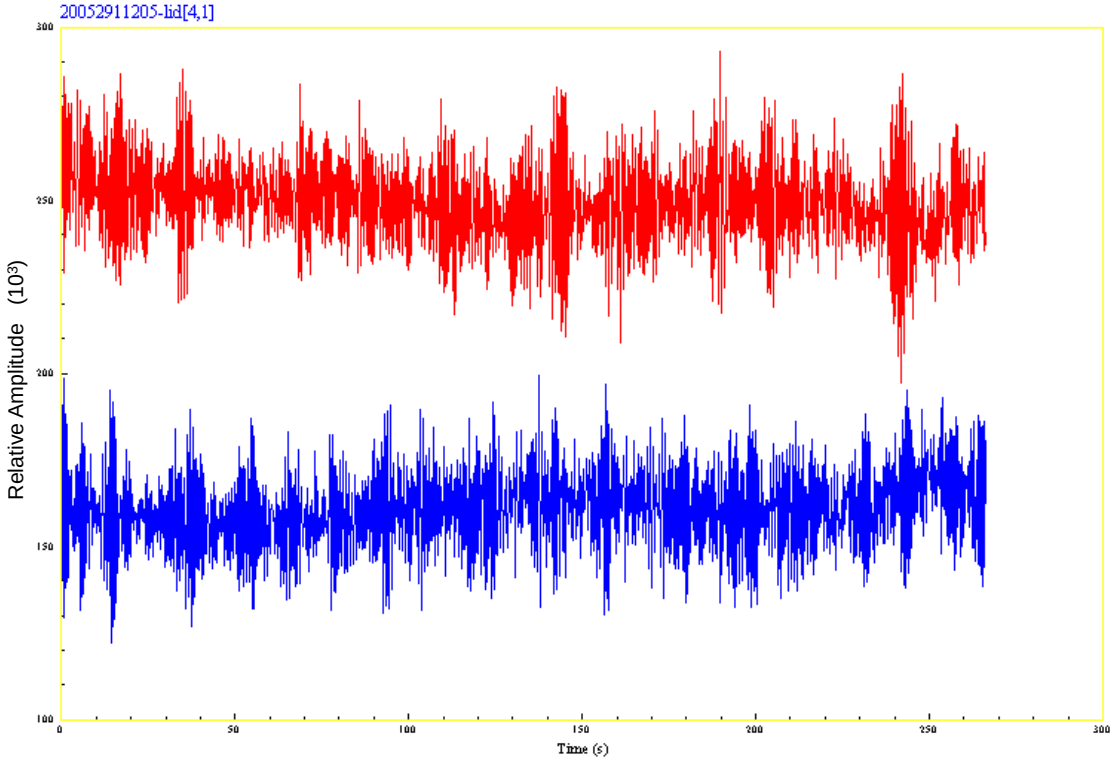

Figure 4.9 Time-Series I (red) and Q (blue) channel for Range-Cell 4, Receive Antenna #1

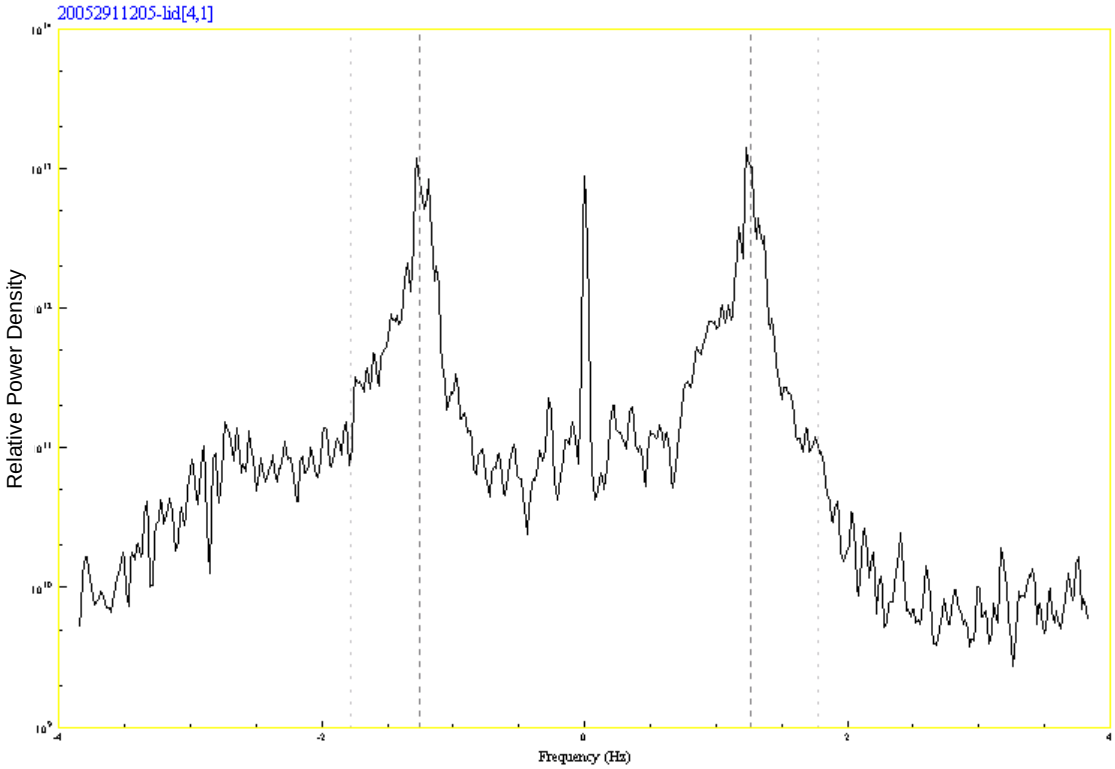

Figure 4.10 Power Spectrum for Range-Cell 4, Receive Antenna #1 (Corresponding to Time-Series shown in Figure 4.9)

4.6 Venice Deployment

The two PortMap radar stations were set up for the 6 week deployment period at the seaward ends of the breakwaters either side of the Lido channel. One station was set up on a mezzanine level of the Punta Sabbioni Lighthouse, the other on a raised concrete block adjacent to the Lido Breakwater Lighthouse. The PortMap electronics and workstation computers were housed inside each of the lighthouses to protect them from moisture and damage from vandalism. Coaxial cables for the antennas together with power and serial communications leads for the motor control were routed from inside the lighthouses out to the antenna systems.

These positions were chosen for their sight lines that encompass an unobstructed view from up the Lido channel through to across and out beyond the channel. This would provide optimal measurement coverage of the channel and the water surrounding each breakwater on the side of the Adriatic sea.

Figure 4.11 PortMap Deployment Locations, Punta Sabbioni (Left) and Lido (Right)

For the system to be able to obtain measurements both inside the channel and out, a steering scheme was adopted such that over a 40 minute period, each station would acquire data from four different boresight directions alternately. In this way, it would be possible to create a complete vector current map that is refreshed every 40 minutes. The timing and directions for this measurement scheme are presented in Table 4.2. Once the end of this sequence is reached, the scheme continually repeats. Over a 24 hour period, 36 acquisitions are recorded for each boresight direction.

Time	Sabbioni Boresight (Master Station)	Lido Boresight (Slave Station)
0	280°	-
5	-	336°
10	220°	-
15	-	36°
20	160°	-
25	-	96°
30	100°	-
35	-	156°

Table 4.2 Antenna Steering Scheme

The projection of these boresight directions onto a satellite image of the channel (Figure 4.12) shows the sequence and coverage zones of this scheme. Although untested, each PortMap radar station is specified to achieve a range of at least 2 km. Regions common in range to both stations dictate the overall system range.

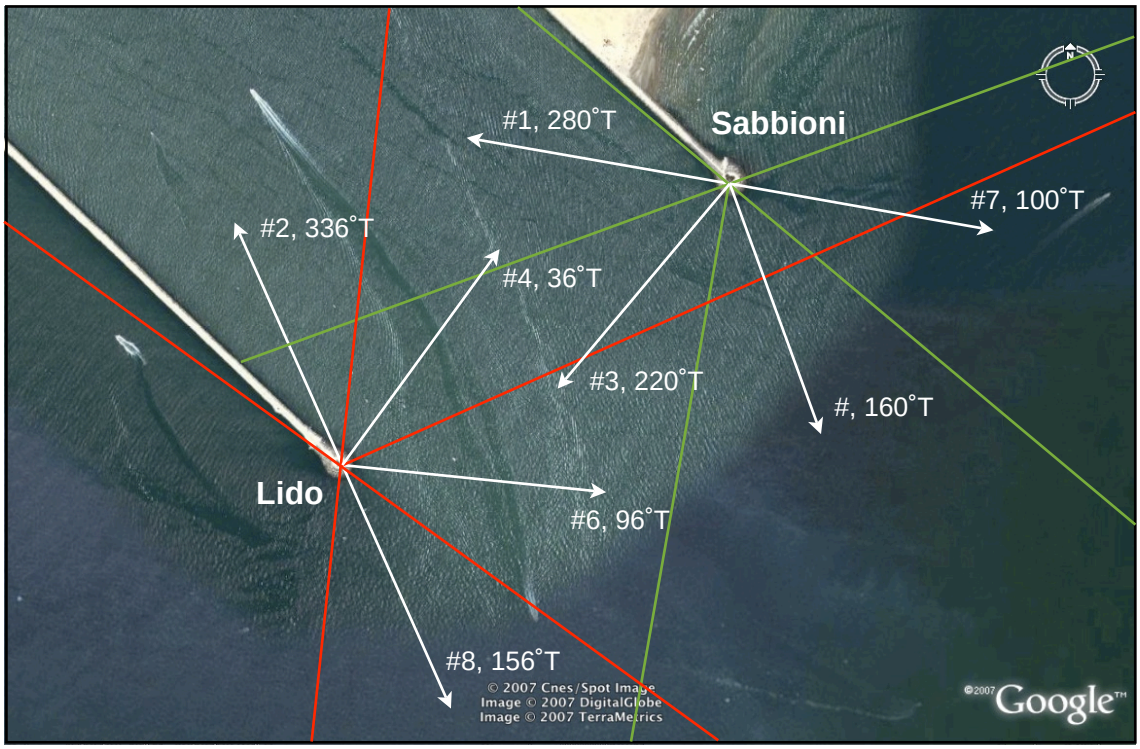

Figure 4.12 Antenna Steering Directions and Sequence
(Image map courtesy of Cnes/Spot, DigitalGlobe, TerraMetrics and GoogleEarth)

A variation to this steering scheme was implemented for three days during the deployment where the radar stations were limited to looking up and across the channel only. Instead of a 40 minute refresh rate of current maps, this would allow updates every 20 minutes.

Time	Sabbioni Boresight (Master Station)	Lido Boresight (Slave Station)
0	280˚	-
5	-	336˚
10	220˚	-
15	-	36˚
20	280˚	-
25	-	336˚
30	220˚	-
35	-	36˚

Table 4.3 Alternative Antenna Steering Scheme